Growth-mediated negative feedback shapes quantitative antibiotic response

S. Andreas Angermayr[1,2,#], Guillaume Chevereau[3], Tobias Bollenbach[1,4*]

[1]Institute for Biological Physics, University of Cologne, Cologne, Germany

[2]Institute of Science and Technology Austria, Klosterneuburg, Austria

[3]INSA de Strasbourg, Strasbourg, France

[4]Center for Data and Simulation Science, University of Cologne, Cologne, Germany

[#]Present address: CeMM Research Center for Molecular Medicine of the Austrian Academy of Sciences, Vienna, Austria.

[*]Corresponding author, t.bollenbach@uni-koeln.de

Abstract

Dose-response relationships are a general concept for quantitatively describing biological systems across multiple scales, from the molecular to the whole-cell level. A clinically relevant example is the bacterial growth response to antibiotics, which is routinely characterized by dose-response curves. The shape of the dose-response curve varies drastically between antibiotics and plays a key role for treatments, drug interactions, and resistance evolution. However, the mechanisms shaping the dose-response curve remain largely unclear. Here, we show in *Escherichia coli* that the distinctively shallow dose-response curve of the antibiotic trimethoprim is caused by a negative growth-mediated feedback loop: Trimethoprim slows growth, which in turn weakens the effect of this antibiotic. At the molecular level, this feedback is caused by the upregulation of the drug target dihydrofolate reductase (FolA/DHFR). We show that this upregulation is not a specific response to trimethoprim but follows a universal trend line that depends only on growth rate, irrespective of its cause. Rewiring the feedback loop alters the dose-response curve in a predictable manner, which we corroborate with a mathematical model. Our results indicate that growth-mediated feedback loops shape drug responses and could be exploited to design evolutionary traps that enable selection against drug resistance.

Introduction

Dose-response curves are a central concept in systems biology and essential for understanding emergent nonlinear phenomena at different scales. A prime example is bacterial gene regulation where cooperativity of transcription factor binding to promoter regions governs the steepness of dose-response curves that characterize gene expression as a function of transcription factor concentration (Bintu *et al*, 2005). The steepness of such transcription factor dose-response curves ultimately determines whether feedback loops in genetic circuits can produce biologically relevant functions such as bistability or oscillations (Elowitz & Leibler, 2000; Gardner *et al*, 2000). At the population level, the bacterial response to antibiotics is captured by similar dose-response curves that quantify the dependence of growth rate on drug concentration. Antibiotic dose-response curves are routinely measured to characterize antibiotic susceptibility via the minimal inhibitory concentration (MIC) or the concentration leading to 50% growth inhibition (IC_{50}), two classic quantities to describe antibiotic efficacy. However, the quantitative shape of the antibiotic dose-response curve – especially its steepness – and its implications are underappreciated.

The steepness of the dose-response curve varies drastically between antibiotics. For many antibiotics, the growth rate drops gradually from high to low as the drug concentration is increased (Fig. 1A); in particular, this is the case for antibiotics targeting DNA replication at the gyrase (e.g. ciprofloxacin) or antibiotics targeting translation at the ribosome (e.g. tetracycline). Beta-lactams like mecillinam (an antibiotic targeting cell wall biosynthesis at a penicillin binding protein) have extremely steep dose-response curves where just a slight relative increase in drug concentration – by about two-fold – causes an abrupt transition from full-speed growth to near-zero net growth (Fig. 1A). At the other end of the spectrum, the folic acid synthesis inhibitor trimethoprim (TMP) has an extremely shallow dose-response curve (Palmer & Kishony, 2014; Rodrigues *et al*, 2016; Russ & Kishony, 2018; Chevereau *et al*, 2015): Reducing growth from full speed to zero with TMP requires a more than 100-fold increase in drug concentration (Fig. 1A). In general, dose-response curves are well approximated by Hill functions and the Hill slope n ("dose-sensitivity") is a quantitative measure of their steepness (Regoes *et al*, 2004; Chou & Talalay, 1983; Chevereau *et al*, 2015): TMP has $n \approx 1.1$, while most antibiotics fall in the range $1.8 \leq n \leq 3.5$, and $n > 6$ (Fig. 1A).

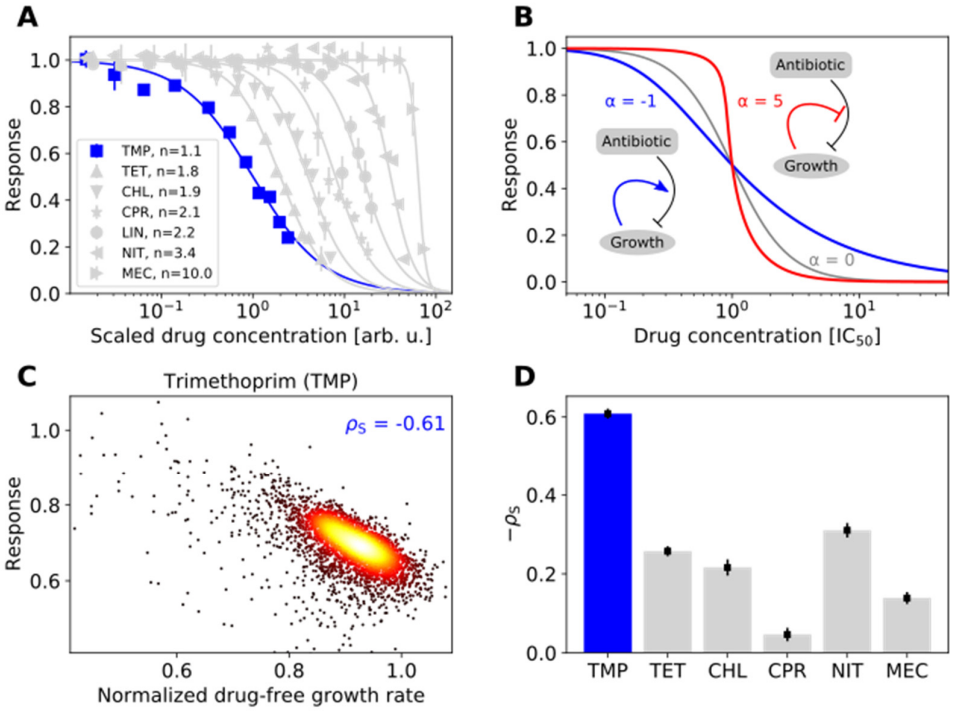

Fig. 1| Trimethoprim exhibits an extremely shallow dose response curve and its efficacy correlates strongly with growth rate. (A) *Dose-response curves (normalized growth rate as a function of drug concentration) for different antibiotics. Growth rate was measured via optical density measurements over time (Methods). Antibiotics used: Trimethoprim (TMP), tetracycline (TET), chloramphenicol (CHL), ciprofloxacin (CPR), lincomycin (LIN), nitrofurantoin (NIT), and mecillinam (MEC). The TMP dose-response curve (dark blue) is by far the shallowest. Lines are fits of the Hill function* $g(c) = \frac{1}{1+\left(\frac{c}{IC_{50}}\right)^n}$ *to the data. Drug concentrations were arbitrarily rescaled to better visualize dose-response curve steepness. Error bars show standard deviation of 12 replicates.* ***(B)*** *Dose-response curves calculated from a mathematical model that captures growth-mediated feedback. Negative feedback (blue) renders the dose-response curve shallower than in the absence of feedback (gray); positive feedback (red) steepens the dose-response curve. Parameters are* $n = 2$, $\alpha = -1$ *for negative feedback and* $\alpha = 5$ *for positive feedback (see main text); drug concentrations are normalized to the* IC_{50} *in the absence of growth mediated feedback (*$\alpha = 0$*).* ***(C)*** *Density scatterplot showing growth response to TMP versus normalized drug-free growth rate for genome-wide gene deletion strains (Baba et al, 2006). These gene deletion strains exhibit diverse growth rates, offering an unbiased way to test the relation between the drug-free growth rate and the response to antibiotics. Response is defined as growth rate in the presence of TMP normalized to the drug-free growth rate of the respective deletion strain. TMP was used at a fixed concentration that inhibits wild type growth by about 30% (Chevereau et al, 2015). Spearman correlation coefficient* ρ_s *is shown.* ***(D)*** *Bar chart showing negative Spearman correlation coefficients* $-\rho_s$ *compared across antibiotics (Supplementary Fig. 1). Error bars show bootstrap standard error of* ρ_s*. TMP (blue) exhibits by far the strongest negative correlation, indicating a growth-mediated negative feedback loop.*

The steepness of the dose-response curve strongly affects the evolution of resistance by spontaneous mutations (Hermsen *et al*, 2012; Chevereau *et al*, 2015). Resistance mutations that slightly increase the MIC provide greater fitness benefits for drugs with a steep dose-response curve compared to drugs with a shallow curve, implying a greater chance to fix in the population. Thus, all else being equal, the rate of resistance evolution for a drug increases with the steepness of its dose-response curve – a trend that is observed in evolution experiments (Chevereau *et al*, 2015). This effect is strongest for drug concentrations near the IC_{50}, which occur for example when populations

83 of motile bacteria evolve resistance in spatial drug gradients (Hol *et al*, 2016; Baym *et al*, 2016).
84 Despite their fundamental relevance for resistance evolution and bacterial responses to antibiotics,
85 the mechanisms that shape the dose-response curve are largely unknown.

86 Feedback loops mediated by growth rate may play a key role in shaping the dose-response curve
87 (Deris *et al*, 2013; Greulich *et al*, 2015). The action of antibiotics affects bacterial growth but the
88 inverse is also true: Slower growing bacteria are less rapidly killed by antibiotics targeting cell wall
89 biosynthesis (β-lactams) (Tuomanen *et al*, 1986; Lee *et al*, 2018) and non-growing (persister) cells
90 are fully protected from many antibiotics (Balaban *et al*, 2004), offering a possibility to evade
91 antibiotic treatments. Slower growth caused by nutrient limitation also affects the bacterial
92 susceptibility to ribosome-targeting antibiotics (Greulich *et al*, 2015). In engineered strains
93 expressing a constitutive resistance gene, a positive feedback loop leads to high dose-sensitivity and
94 even bistability (i.e. co-existence of growing and non-growing cells) in the presence of the ribosome-
95 targeting antibiotic chloramphenicol (Deris *et al*, 2013). Positive feedback occurs as faster growth
96 leads to the upregulation of the resistance enzyme, which in turn enables even faster growth.
97 Growth-mediated feedback loops could more generally explain the drastic differences in dose-
98 sensitivity between antibiotics (Fig. 1A) with positive feedback producing higher (Deris *et al*, 2013)
99 and negative feedback lower dose-sensitivity. However, such feedback loops shaping the dose-
100 response curve of sensitive wild-type bacteria have not yet been characterized.

101 Here, we establish that negative growth-mediated feedback produces an extremely shallow drug
102 dose-response curve. Focusing on TMP, we vary bacterial growth rates by diverse environmental and
103 genetic perturbations and show that slower growth generally lowers the susceptibility of *Escherichia*
104 *coli* to this antibiotic. The molecular origin of this phenomenon lies in the expression of the drug
105 target, which is upregulated in response to TMP but also when growth rate is lowered by other
106 means: TMP lowers growth, which in turn reduces susceptibility to TMP. We show that synthetically
107 reversing this feedback loop can drastically steepen the dose-response curve. The negative feedback
108 loop leads to a seemingly paradoxical situation where adding the antibiotic can even enhance
109 growth under extreme nutrient limitation. Such growth-mediated feedback loops in drug responses
110 could be used to design evolutionary traps that invert selection for resistance.

111

112 **Results**

113 **A minimal mathematical model shows that growth-mediated feedback loops affect the dose-**
114 **sensitivity of drugs**

115 We hypothesized that a growth-mediated negative feedback loop could explain the extreme
116 shallowness of the dose-response curve of TMP (Fig. 1A). As an antibiotic, TMP lowers bacterial
117 growth (by inhibiting dihydrofolate reductase, DHFR, encoded by *folA*). If a lower growth rate in turn
118 protects bacteria from TMP, the dose-response curve should become shallower. To test this idea, we
119 began by developing a mathematical model of bacterial growth in the presence of an antibiotic. We
120 studied a minimal model in which growth-mediated feedback is introduced by making drug efficacy
121 dependent on growth rate. The dose-response curve of antibiotics is captured by a Hill function
122 $g(c) = \frac{g_0}{1+(c/c_0)^n}$, where g_0 is the growth rate in the absence of the drug, n is the dose-sensitivity, c_0
123 is the drug concentration that inhibits growth by 50%, and c is the drug concentration, which is
124 controlled in experiments. To capture effects of growth rate on drug efficacy, we replace c with an
125 effective drug concentration c_{eff} that depends on the externally controlled drug concentration c_{ext}
126 and on the growth rate g, i.e. $c = c_{\mathrm{eff}}(c_{\mathrm{ext}}, g)$. This effective drug concentration captures that the
127 same external concentration can have different effects on the cell, e.g. if the intracellular drug
128 concentration or the expression level of the target is different. The resulting dose-response curve
129 $g(c_{\mathrm{ext}})$ is then implicitly given by

130 $$g = \frac{g_0}{1+\left[\frac{c_{\mathrm{eff}}(c_{\mathrm{ext}},g)}{c_0}\right]^n}. \quad (1)$$

131 Growth-mediated feedback is captured by a function c_{eff} that increases or decreases with the
132 growth rate. For simplicity, we assume that this dependence is linear, i.e. $c_{\mathrm{eff}} = [1 + \alpha\,(1 -$
133 $g/g_0)]c_{\mathrm{ext}}$, where $-1 \leq \alpha < 0$ corresponds to negative and $\alpha > 0$ to positive feedback. Solving
134 equation (1) confirms that negative growth-mediated feedback leads to a shallow dose-response
135 curve (Fig. 1B). In contrast, positive growth-mediated feedback leads to ultrasensitivity (Fig. 1B) and
136 can even produce bistability as previously reported (Elf *et al*, 2006; Deris *et al*, 2013). In this model,
137 the IC_{50} also changes with α: $\mathrm{IC}_{50} = c_0/\,(1 + \alpha/2)$. These theoretical results show how growth-
138 mediated feedback loops can affect the dose-sensitivity of drugs in general.

139

140 **Slower growth generally lowers susceptibility to TMP and steepens its dose-response curve**

141 To test experimentally whether negative growth-mediated feedback underlies the shallow TMP
142 dose-response curve, we varied growth rate in several independent ways and investigated its effect
143 on TMP susceptibility. We first made use of a purely genetic way of varying growth. Specifically, we
144 exploited the growth rate variability resulting from genome-wide gene deletions to expose global
145 trends that are independent of the specific effects of individual gene deletions. Non-essential gene
146 deletions often reduce the drug-free growth rate – some by up to $\sim 50\%$ (Chevereau *et al*, 2015).

147 We re-analyzed a dataset of growth rates of $\sim 4{,}000$ *E. coli* gene deletion mutants under different
148 antibiotics representing common modes of action (Chevereau & Bollenbach, 2015); growth rates
149 were measured at concentrations that inhibit the reference strain by $\sim 30\%$. While each gene can
150 have specific effects for each antibiotic (Nichols *et al*, 2011; Chevereau *et al*, 2015), most genes
151 should be unrelated to the drug mode of action. The global trend of drug susceptibility across all
152 gene deletion strains can thus reveal general consequences of growth inhibition, independent of the
153 specific cellular limitation causing the growth rate reduction.

154 Non-specific growth rate changes caused by gene deletions indicate that slower growth protects
155 *E. coli* from TMP. By correlating the drug-free growth rate of deletion strains with their growth rate
156 in the presence of drugs, we revealed dependencies of drug susceptibility on the drug-free growth
157 rate. The clearest trend emerged for TMP: Its relative effect on growth was weaker in gene deletion
158 strains that had lower growth rates in the absence of drugs (Spearman correlation $\rho_s = -0.6$;
159 Fig. 1C). Compared to other antibiotics, this effect was most pronounced for TMP (Fig. 1D;
160 Supplementary Fig. 1). Slower-growing mutants can even grow at increased TMP concentrations: Full
161 dose-response curve measurements for 78 arbitrary gene deletion mutants showed that the IC_{50} is
162 negatively correlated with the growth rate in the absence of drug for TMP ($\rho_s = -0.27, p = 0.019$)
163 but not significantly correlated for other antibiotics (Supplementary Fig. 2). Thus, TMP represents an
164 extreme case, both in terms of dose-sensitivity and in terms of susceptibility-dependence on growth
165 rate. Overall, these results suggest that slower growth generally lowers the susceptibility to TMP.

166 Slow growth also protects *E. coli* from other antibiotics, but to a far lesser extent. For the prodrug
167 nitrofurantoin (NIT) and the translation inhibitors tetracycline (TET) and chloramphenicol (CHL),
168 there was a weak negative correlation between the drug-free growth rate and that in the presence
169 of the drug ($\rho_s = -0.31$ for NIT, $\rho_s = -0.26$ for TET, $\rho_s = -0.21$ for CHL; Fig. 1D; Supplementary
170 Fig. 1). For the beta-lactam mecillinam (MEC), this trend was even weaker ($\rho_s = -0.14$) and for
171 ciprofloxacin (CPR) almost entirely absent ($\rho_s = -0.05$). Notably, the magnitude of this negative
172 correlation roughly decreases with increasing dose-sensitivity when compared across drugs
173 (Fig. 1A,D). This observation supports the notion that growth-mediated feedbacks are an important
174 contributor to the shape of the dose-response curve for TMP (Fig. 1B) and possibly also for other
175 antibiotics.

176 Reducing growth rate by other means like nutrient limitation or imposing a protein burden also
177 protects *E. coli* from TMP. First, we used glucose limitation in batch culture by adding a non-
178 metabolizable structural analog of glucose, α-methyl glucoside, in varying concentrations to the
179 growth medium. This analog competes with glucose for uptake into the cell, but unlike glucose it

180 cannot be utilized for growth (Hansen *et al*, 1975). Second, we used different carbon sources
181 (glucose, fructose, mannose, glycerol, and galactose) in the growth medium, which is a classic
182 strategy to test for growth-dependent effects (Bremer & Dennis, 2008). Third, we overexpressed a
183 gratuitous protein from an inducible promoter to burden the cells (Dong *et al*, 1995; Scott *et al*,
184 2010). These approaches have different physiological consequences, but they all reduce growth rate
185 in a gradual and controlled manner, while the maximal growth rate and the accessible dynamic
186 range of relative growth inhibition varies between them (Fig. 2). Collectively, they enable us to vary
187 growth rate over a wide range and identify general effects of growth rate, which occur
188 independently of the exact cause of the growth rate reduction. TMP inhibits growth less under
189 glucose limitation: Lowering growth rate by glucose limitation enabled bacteria to grow at slightly
190 increased TMP concentrations (Fig. 2B,C). This trend was even more pronounced when growth was
191 lowered by overexpressing a gratuitous protein – a truncated and inactive version of *tufB* (Dong *et*
192 *al*, 1995) expressed from a synthetic promoter $P_{LlacO-1}$ (Lutz & Bujard, 1997) induced by addition of
193 isopropyl β-D-1-thiogalactopyranoside (IPTG) (Fig. 2D,E,F). Reducing growth by using different
194 carbon sources in a minimal medium could also slightly protect bacteria from TMP, in particular for
195 glycerol (Fig. 2G,H,I). Changing carbon sources has modest effects, presumably because even the
196 highest growth rate (achieved with glucose only) is relatively low and the fold-change in growth is
197 considerably smaller than for glucose limitation (Fig. 2A,D,G). These effects did not occur to a
198 comparable extent for other antibiotics representing common modes of action (Fig. 2C,F,I);
199 however, gratuitous protein overexpression also lowered the susceptibility to mecillinam (MEC),
200 albeit to a lesser extent (Fig. 2F, Supplementary Fig. 6). The effects of growth rate changes were
201 clearly drug-specific and strongest for TMP.

202 Under severe glucose limitation (high ratios of α-methyl glucoside over glucose), which does not
203 support growth, the addition of TMP even rescued bacteria and enabled them to grow again
204 (Fig. 2B). This seemingly paradoxical phenomenon indicates that, under extreme nutrient limitation,
205 the antibiotic TMP can facilitate bacterial growth – perhaps the most drastic illustration of the close
206 interplay between growth rate and TMP susceptibility we observed.

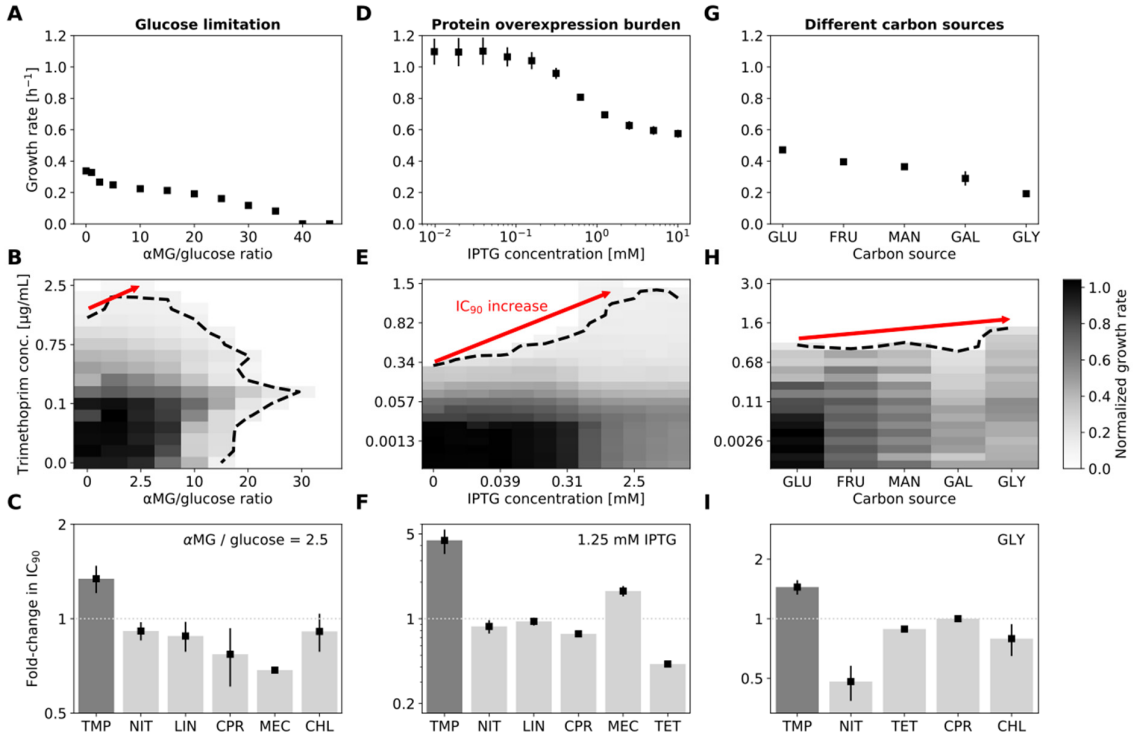

Fig. 2|Slower growth generally lowers the efficacy of trimethoprim. (A) *Growth rate under glucose limitation achieved by adding the non-metabolizable structural glucose analog α-methyl glucoside (αMG) at different ratios to glucose in a minimal medium (Methods).* ***(B)*** *Normalized growth rate (gray scale) from a checkerboard assay in a two-dimensional concentration gradient of TMP and αMG. Dashed black line shows contour line of 90% growth inhibition (IC_{90} line). Red arrow shows increase in IC_{90} as growth is lowered.* ***(C)*** *Fold-change in IC_{90} at αMG/glucose ratio 2.5 in assays as in B for different antibiotics (Supplementary Fig. 5). Lowering growth rate increases IC_{90} for TMP but not for other antibiotics.* ***(D)*** *Growth rate in rich medium (LB) under different levels of overexpression of a gratuitous protein from a T5-lac promoter; overexpression burden is controlled by IPTG concentration (Methods).* ***(E)*** *As B but for growth rate reduction by protein overexpression in a two-dimensional concentration gradient of TMP and IPTG.* ***(F)*** *Fold-change in IC_{90} at 1.25 mM IPTG in assays as in E for different antibiotics (Supplementary Fig. 6). Overexpression of unnecessary protein increases IC_{90} for TMP by almost five-fold; no comparable increase occurs for other antibiotics.* ***(G)*** *Growth rate in minimal medium containing different carbon sources (Methods): Glucose (GLU), fructose (FRU), mannose (MAN), galactose (GAL), and glycerol (GLY).* ***(H)*** *Normalized growth rates (gray scale) on different carbon sources (x-axis) at different TMP concentrations (y-axis).* ***(I)*** *Fold-change in IC_{90} in assays as in H for different antibiotics (Supplementary Fig. 7). Error bars in A, D show standard deviation from eight replicates, those in G from three replicates; day-to-day reproducibility of growth rate measurements is high (Supplementary Fig. 3). Error bars in C,F show standard deviation from three neighboring αMG/glucose ratios and IPTG concentrations centered at 2.5 and 1.25 mM, respectively. IPTG alone has no detectable effect on growth at these concentrations (Supplementary Fig. 4). Error bars in I show standard deviation from three replicates. Antibiotic abbreviations are as in Fig. 1. CHL was not used in the protein overexpression assay in F since the plasmid used for overexpression has a CHL-resistance marker (Methods). Sample growth curves are in Supplementary Fig. 11.*

Lowering growth rate by changing temperature does not show a similar effect: The relative growth reduction by antibiotics remains the same at different temperatures (Supplementary Fig. 8). This is expected since the key physiological parameters that determine growth are invariant under temperature changes (Bremer & Dennis, 2008). This observation indicates that the observed effect has a biological – rather than an elementary physical – origin.

Slower growth increases the steepness of the TMP dose-response curve. We noticed that the extremely shallow dose-response curve of TMP (Fig. 1A) became steeper when growth was slowed

by glucose limitation (Fig. 3A): Halving the growth rate increased the dose-sensitivity from $n \approx 1.1 \pm 0.2$ to $n \approx 1.6 \pm 0.3$ (Fig. 3B). This steepening occurred similarly when growth was slowed by gratuitous protein overexpression (Fig. 3C,D) or by changing the carbon source in the growth medium (Fig. 3E,F). In addition to this change in steepness, the concentration at which TMP starts to have an effect on growth is higher for slower-growing bacteria. However, once the effect of TMP kicks in, the growth rate drops more rapidly with increasing TMP concentration. To better understand this unexpected increase in dose-sensitivity resulting from slower growth, we next aimed to elucidate the underlying mechanism of TMP's growth-rate-dependent action.

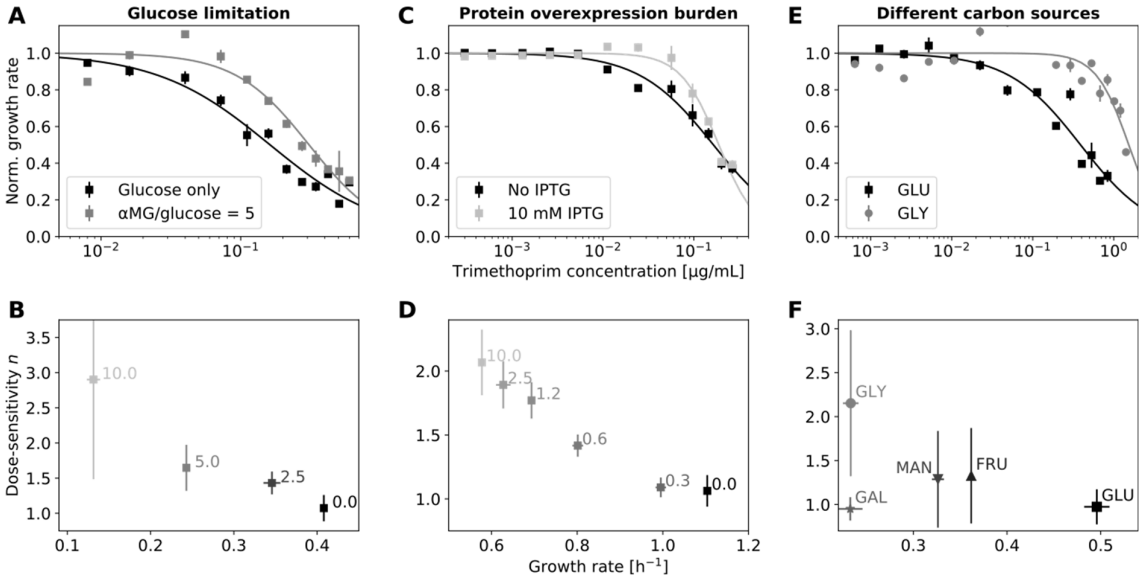

Fig. 3|Slower growth increases the steepness of the trimethoprim dose-response curve. (A) *TMP dose-response curve in minimal medium with glucose as carbon source and at lower drug-free growth rate due to glucose limitation, achieved by increasing the αMG /glucose ratio from 0 (black) to 5 (gray). Glucose limitation results in a steeper dose-response curve. Lines show Hill function fits (cf. Fig. 1A).* ***(B)*** *Steepness of TMP dose-response curves (dose-sensitivity n) versus drug-free growth rate at different αMG concentrations (Methods). Numbers next to data points show αMG/glucose ratio.* ***(C,D)*** *As A,B but for growth limitation by gratuitous protein overexpression in rich growth medium (Methods). Inducing overexpression with IPTG at 10 mM (light gray) steepens the dose-response curve compared to no induction (black). Numbers next to data points in D show IPTG concentration in mM.* ***(E,F)*** *As A,B but for growth limitation by varying the carbon source in a minimal medium (Methods). Carbon sources as in Fig. 2. Growth rate error bars show standard deviation of three replicates; vertical error bars in B,D,F show standard deviation of parameter estimates from Hill function fit.*

Growth-dependent regulation of the TMP drug target leads to a negative feedback loop that flattens the dose-response curve

Regulation of the drug target DHFR could cause the growth-rate-dependent efficacy of TMP. The abundance of the target of TMP (DHFR/FolA) correlates with growth (Bershtein *et al*, 2013); increasing its expression, e.g. by overexpressing *folA* from a plasmid, alleviates the effect of TMP on growth (Palmer & Kishony, 2014). Accordingly, TMP resistance in the lab and in the clinic often

261 evolves by overexpressing *folA*, e.g. by mutating its promoter or by increasing gene copy number
262 (Toprak *et al*, 2012; Nyerges *et al*, 2018; Rood *et al*, 1980; Flensburg & Sköld, 1987; Baym *et al*,
263 2016). These phenomena suggest a plausible mechanism for the reduced susceptibility to TMP at
264 lower growth rates: We hypothesized that slower growth generally leads to increased *folA*
265 expression, which in turn partially protects bacteria from TMP (Soo *et al*, 2011; Palmer & Kishony,
266 2014) – a buffering mechanism against inhibition of FolA.

267 DHFR expression increases similarly in response to TMP and to other means of reducing growth rate.
268 Using a promoter-GFP reporter (Methods), we confirmed that *folA* expression increases in response
269 to TMP (Fig. 4A), as previously observed in whole populations (Bollenbach *et al*, 2009; Bershtein *et*
270 *al*, 2015; Rodrigues *et al*, 2016) and single cells (Mitosch *et al*, 2017). However, we noticed that *folA*
271 expression increases similarly when growth is slowed by glucose limitation (Fig. 4B). This observation
272 suggests that the upregulation of *folA* under TMP is not a specific response to target inhibition, but
273 rather a general response to reduced growth rate. Expression levels of constitutive genes are
274 generally expected to increase when the quality of the nutrient environment is lowered (Scott *et al*,
275 2010). While the *folA* promoter can be regulated by two transcription factors (TyrR (Yang *et al*, 2007)
276 and IHF (Keseler, 2004)) under certain conditions, it behaved similarly to a constitutive promoter in
277 these experiments. Indeed, *folA* expression across a two-dimensional concentration gradient of TMP
278 and the glucose analog varied (Supplementary Fig. 9) but was largely determined by growth rate
279 alone (Fig. 4C). Like constitutively expressed genes (Scott *et al*, 2010), *folA* expression followed a
280 general, approximately linear increase with decreasing growth rate, approaching a fixed maximum
281 level at zero growth (Fig. 4C). Since increased *folA* expression protects bacteria from TMP (Palmer &
282 Kishony, 2014), this mode of regulation results in a negative growth-mediated feedback loop: TMP
283 inhibits growth, which leads to the upregulation of its target, thereby attenuating its own efficacy.

284 Saturating growth-dependent regulation of the drug target can explain the steepening of the dose-
285 response curve at lower growth rates. Higher drug target expression at lower growth rates can
286 compensate for some of the target inhibition caused by TMP. This offers a plausible explanation as
287 to why the effect of TMP becomes apparent only at higher concentrations when the drug-free
288 growth rate is lower (Fig. 2). But how does slower growth steepen the TMP dose-response curve
289 (Fig. 3)? We noticed that *folA* expression at different drug-free growth rates converges to a fixed
290 value when TMP is added (Fig. 4D). In other words, the relative upregulation of *folA* in response to
291 TMP gets weaker with decreasing drug-free growth rate; it even disappears completely at the
292 highest glucose-analog concentrations (Fig. 4D). This convergence of *folA* expression in different
293 conditions may reflect that the promoter reaches its maximal induction level. At lower drug-free
294 growth rates, the promoter is already near its maximum expression level without TMP and saturates

quickly when TMP is added, resulting in weaker relative upregulation than at higher growth rates. Consistent with this scenario, increasing *folA* expression at low growth rates is deleterious (Supplementary Fig. 10). Thus, lower drug-free growth rates weaken – or even break – the growth-mediated negative feedback loop, resulting in steeper dose-response curves.

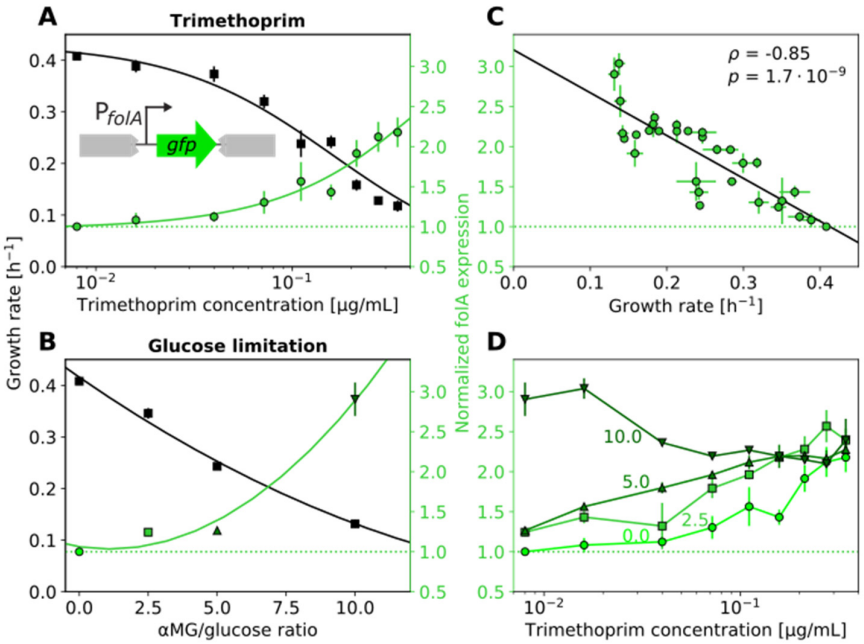

Fig. 4|Slower growth increases folA expression, irrespective of whether growth is reduced by trimethoprim or by nutrient limitation. (A) *Dependence of growth rate (black) and folA expression (green) on TMP concentration. Schematic: FolA expression was measured using a promoter-GFP reporter inserted at a neutral site in the genome (Methods).* ***(B)*** *Growth rate (black) and folA expression (green) in the absence of TMP at different growth rates achieved by different ratios of αMG/glucose.* ***(C)*** *Scatterplot of folA expression level with growth rate across all combinations of TMP concentrations and αMG/glucose ratios shown in A and B (Supplementary Fig. 9). Pearson's correlation coefficient ρ and p-value are shown.* ***(D)*** *Dependence of folA expression on TMP concentration at four different αMG/glucose ratios (0, 2.5, 5, and 10 as shown). Darker green indicates greater αMG/glucose ratio. FolA expression converges approximately to the same level at high TMP concentrations. Black line in A shows Hill function fit as in Fig. 1A; other lines show polynomial fits of first (C) or second order (A,B) to guide the eye. Horizontal dotted green line shows folA expression level in the absence of TMP. Error bars show standard deviation of three replicates.*

Artificially breaking the growth-mediated feedback loop steepens the TMP dose-response curve

To corroborate that the shallowness of the TMP dose-response curve is due to a growth-mediated negative feedback loop, we aimed to break this loop even under nutrient conditions that support high drug-free growth rates. To this end, we constructed a synthetic strain in which the expression of *folA* from its endogenous locus is controlled by an inducible promoter. We used a strain allowing IPTG-mediated induction of *folA* and *folA-gfp,* respectively, with an expression level in the same range as wild-type *folA* (Methods). Note that this alone does not eliminate the feedback loop since,

at constant inducer levels, expression from the inducible promoter can change with growth rate, similar to expression from the endogenous *folA* promoter. Nevertheless, we can use this synthetic strain to infer the shape of the TMP dose-response curve at constant *folA* expression by continuously varying the inducer concentration and measuring FolA levels. Specifically, we measured growth rate and *folA* expression using a FolA-GFP fusion protein across a two-dimensional concentration gradient of TMP and inducer (Fig. 5A; Methods). We then determined the growth rate as a function of TMP concentration on a path through this two-dimensional concentration space along which *folA* expression is constant. The resulting TMP dose-response curve at constant *folA* expression is steeper than in wild type ($n = 2.0 \pm 0.3$; Fig. 5B,C). It becomes even steeper for a positive feedback loop, which is inferred from a path through the two-dimensional concentration space along which *folA* expression decreases with increasing TMP concentration ($n = 5.0 \pm 0.9$; Fig. 5B,C). These results provide direct evidence that a negative growth-mediated feedback loop implemented by the regulation of the drug target causes the exceptional shallowness of the TMP dose-response curve.

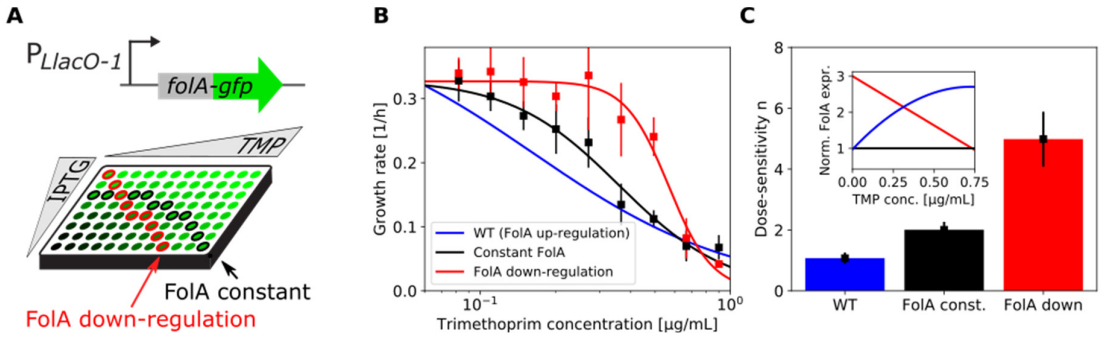

Fig. 5|Breaking the growth-mediated negative feedback loop steepens the trimethoprim dose-response curve. (A) *Schematic: FolA expression is controlled by varying the IPTG concentration and measured by flow cytometry using a GFP fusion to FolA. Shades of green indicate different FolA expression levels. Wells encircled in red indicate how the effect of FolA down-regulation with increasing TMP concentration can be inferred; wells encircled in black illustrate the same for constant FolA expression.* ***(B)*** *Growth rate as a function of TMP concentration for different paths through IPTG-TMP concentration space as illustrated in A (Methods). Constant FolA is shown in black and FolA down-regulation in red. Wild type dose-response curve (blue line; fit from Fig. 4A) is shown for comparison.* ***(C)*** *Steepness of the dose response curve (quantified as dose-sensitivity n) for the three cases in B. Inset: Normalized FolA expression level as a function of TMP concentration for the three cases in B; WT (blue) shows fit from Fig. 4A; colors as in the bar chart and in B. Error bars in B show standard deviation of the measured growth rates used for interpolating the values shown (Methods). Error bars in C show standard deviation of parameter estimates from Hill function fit.*

Discussion

We showed that slower-growing bacteria are generally less affected by TMP, largely regardless of what causes their slower growth (Fig. 2). This phenomenon implies a growth-mediated negative feedback loop, which causes TMP's extremely shallow dose-response curve (Fig. 1A): TMP lowers growth, which in turn weakens the inhibitory effect of the drug. Mechanistically, this feedback loop

351 is rooted in the expression level of the drug target DHFR, which is upregulated with decreasing
352 growth rate (Fig. 4). Elimination or inversion of this feedback loop from negative to positive
353 drastically steepens the dose-response curve (Fig. 5). Together with recent work on ribosome-
354 targeting antibiotics (Deris *et al*, 2013), these results support a general role of growth-mediated
355 feedbacks in shaping antibiotic dose-response curves (Fig. 1B).

356 Consistent with this view, the steepness of the dose-response curve of antibiotics representing
357 different modes of action correlates roughly with the decrease in drug susceptibility under slower
358 growth (Fig. 1A,D). In particular, while their effect is less extreme than for TMP, the ribosome
359 inhibitors CHL and TET also exhibit relatively low dose-sensitivity and slightly reduced susceptibility
360 under slower growth (Fig. 1D, Supplementary Fig. 1). The mechanism underlying this weaker growth-
361 mediated negative feedback for CHL and TET resembles that for TMP since their drug target, the
362 ribosome, is upregulated in response to these drugs (Scott *et al*, 2010)—similar to DHFR in response
363 to TMP. The prodrug NIT is an outlier: It has a relatively steep dose-response curve (Fig. 1A) despite
364 being less susceptible under slower growth (Fig. 1D). This may be caused by additional (unknown)
365 mechanisms acting on top of the growth-mediated feedback we focus on here. Identifying the
366 molecular mechanisms underlying feedback loops or other phenomena that shape dose-response
367 curves will likely require detailed studies for each antibiotic or antibiotic class.

368 By using a mathematical model in which the effective drug concentration is growth-rate dependent,
369 we showed that growth-mediated feedbacks generally affect the shape of the dose-response curve.
370 For TMP, the effective drug concentration is reduced due to the upregulation of DHFR: The same
371 concentration of TMP has a weaker effect on growth at higher intracellular concentrations of DHFR.
372 For simplicity, we assumed that the effective drug concentration changes linearly with the growth
373 rate. This is in line with the experimental observation that DHFR is upregulated linearly with
374 decreasing growth rate, approaching a maximum at zero growth (Fig. 4C). Decoupling the DHFR level
375 from the growth rate by forcing it to a constant value, or even to decrease in response to TMP,
376 results in a steeper dose-response curve (Fig. 1B) in agreement with experimental observations
377 (Fig. 5B,C). The model further helps to rationalize why dose-response curves become steeper when
378 the drug-free growth rate is decreased, corresponding to a poorer nutrient environment. At very low
379 drug-free growth rates, the DHFR level becomes almost constant (Fig. 4D), effectively breaking the
380 negative feedback loop and thus steepening the dose-response curve, as observed experimentally
381 (Fig. 3). Note, that our model can explain relative changes in dose-sensitivity but it remains
382 challenging to explain its absolute value. Indeed, all antibiotics we studied have dose-sensitivities
383 $n > 1$ and most have $n > 2$ (Fig. 1A), which requires additional nonlinearities beyond the growth-
384 mediated one we focused on here, e.g., in the kinetics of antibiotic transport and target binding.

385 Explaining the absolute values of the dose-sensitivities for different drugs remains a challenge for
386 future work.

387 We observed that an artificial nutrient limitation that results in no or extremely slow growth can be
388 alleviated by adding the antibiotic TMP (Fig. 2B). This indicates that bacteria may not regulate DHFR
389 expression in a way that maximizes growth under extreme nutrient limitation. Indeed, slow growth
390 in these conditions coincides with high *folA* expression (Fig. 4D). High *folA* expression is deleterious
391 (Bhattacharyya *et al*, 2016) as cellular resources are diverted toward excessive folic acid synthesis.
392 Consistent with this view, TMP facilitated bacterial growth when *folA* was overexpressed to levels
393 that were deleterious in the absence of TMP (Supplementary Fig. 10). Together, these observations
394 show that DHFR level is the main driver of TMP susceptibility and suggest that costly overproduction
395 of DHFR, which can be rescued by adding TMP, occurs under extreme nutrient limitation. Since TMP
396 increases the fitness of bacteria that evolve under extreme nutrient limitation, the usual selection
397 pressure for antibiotic resistance is inverted under such conditions: Mutations that usually enhance
398 TMP action (e.g. increased drug uptake) can be selected. Similar to certain drug combinations (Chait
399 *et al*, 2007), this situation provides an opportunity to select against antibiotic-resistant bacteria. One
400 potential advantage of creating such conditions with a sugar analog instead of a second drug is that
401 bacteria can hardly evolve resistance to such an analog, as impaired sugar uptake would come at a
402 massive fitness cost.

403

404 **Methods**

405 **Growth conditions and growth rate measurements**

406 Unless otherwise noted the chemicals used were from Sigma-Aldrich (Steinheim, DE). The growth
407 medium used was either LB Broth Lennox (L3022), pH set to 7.0 with NaOH before autoclaving, or
408 M9 minimal medium made from $Na_2HPO_4.7H_2O$ (Fisher Scientific Acros Organics 206515000), KH_2PO_4
409 (P9791), NaCl (S3014), and NH_4Cl (A9434)) supplemented with 0.1 mM CaCl2 (Fluka 223506), 2mM
410 MgSO4 (M7506), and 0.001% (v/v) Triton-X 100 (T8787). Triton-X was added to flatten the meniscus
411 that forms in 96-well pates (Mitosch *et al*, 2017). Carbon sources in the M9 medium were glucose
412 (G8270), glycerol (VWR 0854), mannose (Carl Roth 4220.2), fructose (F0127), galactose (G0750), all
413 of which were added at 0.4% (w/v) and prepared as filter sterilized 20% (w/v) stock solutions stored
414 at room temperature in the dark. Experiments were started from a frozen glycerol stock. Bacteria
415 were streaked on an LB agar (L2897) plate (containing antibiotics as appropriate) incubated
416 overnight at 37°C and a single colony was inoculated in 2 ml of the appropriate growth medium

417 (containing antibiotics if appropriate) and grown for about 20 h to obtain a pre-culture that has
418 reached stationary phase. We inoculated experimental cultures with a 1000-fold dilution from a
419 stationary phase culture when growth was determined by optical density measurements at 600 nm
420 (OD_{600}). For the experiments with luminescence-readout, the pre-culture was grown in 20 ml LB
421 medium in a 250 ml flask until stationary phase; 100 μl aliquots were transferred to the wells of a
422 96-well plate, supplemented with glycerol to 15% and frozen at -80°C. To start a luminescence-based
423 experiment the plate was thawed, and dilutions were performed in 96-well plates with fresh
424 medium using pin tools (VP407 and VP408, V&P Scientific Inc., CA, USA), which transfer 1.5 μl and
425 0.2 μl per well, respectively. Subsequent use resulted in a 10^7-fold dilution from a stationary phase
426 culture. In all cases, the pre-cultures were incubated at 30°C with a shaking speed of 250 rpm
427 (Innova 44, Eppendorf New Brunswick, DE).

428 Pre-cultures carrying plasmids and cultures needed for molecular cloning procedures were prepared
429 with antibiotics at the following concentrations: chloramphenicol 35 μg/ml (C0378), kanamycin
430 25 μg/ml (K4000), ampicillin 50 μg/ml (A9518), spectinomycin 100 μg/ml (S6501).

431 Unless otherwise noted antibiotics were dissolved in ethanol (32221). Stock solutions in water were
432 filter-sterilized. Aliquots of stocks were stored at -20°C in the dark. The antibiotics used were
433 trimethoprim (92131), nitrofurantoin (N7878), chloramphenicol (C0378), lincomycin (dissolved in
434 water, 62143), mecillinam (dissolved in water, 33447), tetracycline (268054), and ciprofloxacin
435 (dissolved in water, 17850). IPTG (VWR 437144N) was added to cultures to control expression from
436 IPTG-responsive promoters ($P_{T5\text{-}lac}$, $P_{LlacO\text{-}1}$) (Kitagawa *et al*, 2005; Lutz & Bujard, 1997). A filter-
437 sterilized solution of 1M IPTG in water served as stock solution. IPTG was stored at -20°C in the dark
438 and aliquots were thawed at room temperature before use. For the non-metabolizable glucose
439 analog α-methyl glucoside (M9376), which competes for glucose uptake and essentially imposes
440 glucose limitation (Hansen *et al*, 1975), a filter sterilized solution of 50% (w/v) in M9 salts served as
441 stock solution.

442 The experiments shown in Fig. 1-3 were performed using a robotic system as described
443 previously (Chevereau *et al*, 2015) and have a day-to-day variability (coefficient of variation, CV) of
444 growth rate for unperturbed cultures of less than 5% (Ref. (Chevereau *et al*, 2015) and
445 Supplementary Fig. 3). The experiments shown in Fig. 4 and 5 were performed using two plate
446 readers: A Synergy Neo2 and a Synergy H1 (both from Biotek Inc., VT, USA). Both were set to 30°C
447 with continuous shaking at an orbital displacement of 1 mm and a speed of 807 rpm, and after a
448 settling period of 10 seconds the optical density at 600 nm and GFP fluorescence were measured
449 every 10 min. Flat transparent microtiter plates (Nunc Thermo Scientific FT 96-well, 236105) with

450 lids were used. The experiments presented in Supplementary Fig. 8 were performed using an Infinite
451 M1000 Pro plate reader (Tecan Inc., CH) equipped with an integrated stacking module. The stack
452 was housed in a custom-built (IST Austria Miba Machine Shop, Klosterneuburg, AT) acrylic glass box
453 equipped with a custom-built heating block, a thermostat and strong ventilation to assure a
454 homogenous temperature over the plates and the stack (Kavčič *et al*, 2020). For these experiments
455 (Supplementary Fig. 8), the wild-type strain used here (*E. coli* BW25113) was transformed with a
456 kanamycin resistance-bearing plasmid (pCS-λ) carrying luciferase genes used to determine the
457 growth rate (Kishony & Leibler, 2003; Chait *et al*, 2007). For the actual growth experiments
458 kanamycin was omitted; however this was not a problem as the plasmid is retained throughout the
459 duration of such an experiment (Kavčič *et al*, 2020). Luminescence assays were performed using flat
460 white microtiter plates (Nunc Thermo Scientific FW 96-well, 260860). These plates were sealed with
461 a transparent foil (TopSeal-A Plus, PerkinElmer) and about ten plates were used per stack.
462 Luminescence was measured every 10 to 20 min. Before each measurement, plates were shaken for
463 10 sec at 582 rpm with a 1 mm amplitude. The culture volume per well was 150 µl. The day-to-day
464 CV for unperturbed cultures for the growth rate in the luminescence-setup was 3%.

465 The growth rate was determined by a linear fit of the log-transformed and background-subtracted
466 OD_{600} from the exponential growth phase of the cultures using custom Matlab (R2016b, MathWorks
467 Inc.) scripts. To capture the exponential growth phase for cultures in LB we used background-
468 subtracted OD_{600} windows of 0.02 to 0.2 and for minimal medium 0.03 to 0.12; these windows cover
469 one order of magnitude and at least two doublings and take the lower growth yield in minimal
470 medium into account. The lowest accepted growth rate for LB was 0.1 h^{-1} and for minimal medium
471 0.03 h^{-1}, both corresponding to about 10% of the respective unperturbed maximal growth rate. For
472 the Hill function fits in Fig. 3C,D, growth rates below 0.2 h^{-1} were ignored because too many data
473 points fell in this range at higher IPTG concentrations (Fig. 2E) – these data points would thus
474 dominate the fit, which is undesirable since they contain less information about the shape of the
475 dose-response curve (i.e. the dose-sensitivity). The duration of experiments for LB cultures was
476 about 22 h, for minimal medium about 46 h. For all experiments performed in LB medium, data after
477 $\sim 1{,}000$ min were discarded to avoid the inclusion of faster growing mutants which occurred
478 sporadically in the presence of antibiotics; this was not necessary for experiments in minimal
479 medium. To capture the growth rate strictly during exponential phase from the luminescence-based
480 experiments, the rate of luminescence increase was determined by a linear fit of the log-
481 transformed data between 10^2 cps and 10^5 cps.

482

483 **Expression level measurements using plate readers**

484 Two plate readers Synergy Neo2 and a Synergy H1 (see section *Growth conditions* for further details)
485 were used for GFP fluorescence measurements. The filter set used in the Neo2 provided excitation
486 at 485nm (BW20) and emission at 516nm (BW20) (Biotek fluorescent filter #105). The settings for
487 the monochromator-based H1 model were 485 nm for excitation and 528 nm for emission. Both
488 readers produced consistent values and results. The measured values for experiments where both
489 plate readers were used in parallel were adjusted accordingly (i.e. simply normalized by a constant
490 obtained from measuring the same sample on both readers). The expression level was determined
491 essentially as described (Zaslaver *et al*, 2006; Mitosch *et al*, 2017). Briefly, for each GFP-expressing
492 strain, a similar strain without GFP-expression was grown in parallel in the same conditions (see
493 section *Strain construction* for further details). For both strains the exponential growth phase was
494 determined and the background subtracted GFP-signal from the GFP-less strain was subtracted from
495 the GFP-carrying strain for cultures with similar growth rates and at the same OD_{600}. As the exact
496 same OD_{600} values were mostly not met, linear interpolation (Matlab function *interp1*) was used to
497 generate an interpolated GFP-value between the two GFP values of the two nearest OD_{600} values.
498 The expression level is obtained from the slope of a linear fit (Matlab function *fit*) to the GFP over
499 OD_{600} data during exponential growth. In the experiments using the strains with the reporter
500 construct with the native promoter (BWAA01, Fig. 4), fast-folding GFP (Zaslaver *et al*, 2006) was used
501 whereas in the experiments with the synthetic IPTG-inducible promoter construct (BWAA29R1, Fig.
502 5) the GFP from the ASKA-library (Kitagawa *et al*, 2005) was used.

503

504 **Expression level measurements using flow cytometry**

505 For the expression level determination of the strains with IPTG-induced *folA-gfp* expression (Fig. 5)
506 we used a combination of plate readers (Biotek Synergy H1) for optical density measurements for
507 growth rate determination (see section growth rate measurements for details) and flow cytometry
508 (Beckman Coulter CytoFLEX B2-RQ-V2 with 96-well plate module) for fluorescence measurements.
509 Flow cytometry was used because of its higher signal-to-noise ratio compared to fluorescence
510 measurements on plate readers. Strains were grown in the plate readers and growth was monitored
511 by measuring optical density every 10 min. When strains were in mid-exponential growth phase (OD
512 $\sim$ 0.1), they were diluted 1,000-fold in ISOTON II (Beckman Coulter) and measured immediately on
513 the flow cytometer. Gating in SSC-A and GFP FITC-A channels in the flow cytometry analysis software
514 (Beckman Coulter Cytexpert 2.3.0.84) allows finding of (fluorescent) cells and determination of the
515 mean and relative coefficient of variation of fluorescence intensity. Strains used were BWAA11,

516 BWAA 12, BWAA 19R1, and BWAA 20R1 (see section *Strain construction* for details) and TMP and
517 IPTG gradients starting at 0.9 µg/ml and 2.5 mM were applied, respectively. Growth rates at
518 constant or decreasing FolA expression level were calculated by linear interpolation of the growth
519 rates measured at different IPTG and TMP concentrations as illustrated in Fig. 5A.

520

521 **Strains and strain construction**

522 We used *E. coli* BW25113 and several derivatives thereof. BW25113 is the parent strain of the KEIO
523 collection, a widely used whole-genome deletion mutant collection (Baba *et al*, 2006). For the
524 overexpression experiments, BW25113 was transformed with the necessary plasmids (Table 1)
525 which stem from the ASKA-library, a plasmid-based whole-genome overexpression
526 collection (Kitagawa *et al*, 2005). To reduce growth rate by gratuitous protein expression we used a
527 truncated elongation factor Tu (EF-Tu, *tufB*) as previously done for a similar purpose (Dong *et al*,
528 1995). Briefly, starting with the ASKA-library plasmid carrying *tufB*, the SmaI restriction fragment of
529 243 bp in length was cut out and the blunt-ended DNA fragment was closed by ligation to form a
530 plasmid again, named pAAtufB here. This deletion results in a shortened, non-functional gene
531 (*ΔtufB*), which can be used to provide gratuitous protein expression, resulting in a burden that slows
532 down growth (Dong *et al*, 1995; Scott *et al*, 2010). The plasmids from the ASKA-library (Kitagawa *et*
533 *al*, 2005) use the $P_{T5\text{-}lac}$ promoter, which allows for a graded control of expression by the addition of
534 the inducer IPTG (which works sufficiently well in a *lac*-operon compromised strain like *E. coli*
535 BW25113). As control, we used pAA30 which is the empty ASKA plasmid modified to not contain a
536 gene to prevent any expression; we created this plasmid since the original empty ASKA plasmid does
537 in fact encode a short coding sequence in frame with the promoter. Briefly, through a PCR with
538 overlapping primers (for general strategy see (Heckman & Pease, 2007; Hansson *et al*, 2008)) (Fw:
539 CATTAAAGAGGAGAAATTAACTGGGTCGACCTGCAG, Rv:
540 CTGCAGGTCGACCCAGTTAATTTCTCCTCTTTAATG) a short stretch of pCA24N(-) encompassing start
541 codon over the His-Tag and until the stop codon, was eliminated. The elimination was confirmed by
542 sequencing the resulting plasmid with primers flanking the gene insertion site (Fw:
543 CAACAGTTGCCTAAGAAACCAT, Rv: TGAGGTCATTACTGGATCTATCAAC). For the strong *folA*
544 overexpression the ASKA plasmid pCA24N(-)folA was used.

545 We generated reporter strains and a strain with inducible *folA* regulation. To construct the first *gfp*-
546 reporter and corresponding *gfp*-less control pair integrated into the chromosome (BWAA01 and
547 BWAA02), the promoter-reporter construct for P_{folA} and the corresponding region from the empty
548 plasmid pUA66 from the reporter library (Zaslaver *et al*, 2006) were integrated into a neutral site

549 (*phoA*) in the genome, respectively. To this end, P1 transduction was used to move the construct
550 from an MG1655 strain carrying the reporter constructs (Bollenbach *et al*, 2009) into the BW25113
551 background. The insertion was confirmed by sequencing PCR products generated using primers
552 binding outside the *phoA* locus (Fw: GGCGCTGTACGAGGTAAAG, Rv: GGGTTAAAGTTCTCTCGGCA).

553 The other reporters were based on *folA-gfp* fusion constructs from the ASKA-library (Kitagawa *et al*,
554 2005). Again, pairs of strains were made where each pair consists of a strain with and a strain
555 without the *gfp* fused to *folA*. We generated several pairs to induce and thereby control expression
556 level by an IPTG-responsive promoter ($P_{LlacO-1}$ (Lutz & Bujard, 1997)) and one pair with the native
557 regulation through P_{folA}. This was done to approximately match the induced expression with the level
558 of the native regulation. We generated strains with the inducible $P_{LlacO-1}$ promoter with five different
559 ribosome binding sites of different strength with the sequences (RBS1, 3, 4, 5, and 6) originating
560 from (Deris *et al*, 2013). Those strains were compared to strains with the native regulation (BWAA11
561 and BWAA12) which were made in parallel according to a similar strategy as described below. Based
562 on similar expression levels for BWAA19R1 and BWAA11, BWAA19R1 with RBS1, was chosen for the
563 experiment shown in Fig. 5. To create the *gfp* fusion strains, *folA-chlR* and *folA-gfp-chlR* fragments
564 were PCR-amplified from the *folA*-carrying ASKA-library plasmids (using as template the respective
565 plasmids from the library, with and without *gfp* (Kitagawa *et al*, 2005)) as a first step and were used
566 for recombineering (Datsenko & Wanner, 2000) into the plasmid pKD13-gfpmut3 (a derivative of
567 pKD13 (Datsenko & Wanner, 2000); gift from Bor Kavčič). Primers used were
568 CAGCAGGACGCACTGACCGAATTCATTAAAGAGGAGAAAGGTACCGCATGATCAGTCTGATTGCGGCGTTAG
569 and GACTGAGCCTTTCGTTTTATTTGATGCCTCTAGACTCAGCTAATTAAGCGTAGCACCAGGCGTTTAAGG.
570 This resulted in pAA39 and pAA40 where an FRT-flanked kanamycin resistance cassette, the
571 promoter $P_{LlacO-1}$ driving *folA* and the *folA-gfp* fusion, respectively, and a chloramphenicol resistance
572 cassette are present (in this order). These plasmids first served as source for the promoter-*folA* and
573 *folA-gfp* fusion with a chloramphenicol resistance cassette to be inserted into the genome at the
574 *folA* locus to generate the strains with the native regulation (BWAA11 and BWAA12). PCR-fragments
575 for recombineering were obtained with the previously used forward primer
576 CAGCAGGACGCACTGACCGAATTCATTAAAGAGGAGAAAGGTACCGCATGATCAGTCTGATTGCGGCGTTAG
577 and AAGACGCGACCGGCGTCGCATCCGGCGCTAGCCGTAAATTCTATACAAAACTAGACTCAGCTAATTAAGC
578 serving as reverse primer to get the *folA* gene with and without *gfp,* respectively, and the
579 chloramphenicol resistance cassette (but not the synthetic promoter) were inserted into the
580 genome of BW25113 replacing the *folA* gene (but not the promoter on the genome). Next, by
581 recombineering with PCR-fragments containing the kanamycin resistance cassette only obtained
582 with the primers

583 GTGATACGCCTATTTTTATAGGTTAATGTCATGATAATAATGGTTTCTTAGAAGTTCCTATTCTCTAGAAAGTAT
584 AGG and
585 AAGACGCGACCGGCGTCGCATCCGGCGCTAGCCGTAAATTCTATACAAAAGTGTAGGCTGGAGCTGCTTC
586 from pKD13-gfpmut3 the chloramphenicol resistance cassette was replaced with the FRT-flanked
587 kanamycin resistance cassette. Next, to obtain a marker-less strain the kanamycin resistance
588 cassette was removed using the plasmid pCP20, as described (Cherepanov & Wackernagel, 1995).
589 For the strains with the IPTG-inducible regulation (BWAA19R1 and BWAA20R1) a similar strategy
590 applied. Primers
591 AACATACCGGCAACATGGCGGATGAACCGGAAACGAAACCCTCATCCTAAGTGTAGGCTGGAGCTGC and
592 TCCATGCCGATAACGCGATCTACCGCTAACGCCGCAATCAGACTGATCATGCGGTACCTTTCTCCTCTTT
593 (putative RBS1 sequence from (Baba *et al*, 2006) underlined) were used to amplify the FRT-flanked
594 kanamycin resistance cassette, the promoter $P_{LlacO-1}$ driving *folA* and the *folA-gfp* respectively of
595 pAA39 and pAA40 (but not the chloramphenicol resistance cassette). Next, to obtain a marker-less
596 strain the kanamycin resistance cassette was removed using pCP20. All four marker-less strains were
597 further modified by P1 transduction from a MG1655 strain carrying the *lacI* gene under the
598 promoter P_{lacO1} and a FRT-flanked kanamycin resistance cassette at the neutral insertion site *intS*
599 (based on the strain from (Garcia *et al*, 2011) (HG105) and a gift from Bor Kavčič). The insertion was
600 confirmed by sequencing PCR products generated using primers binding outside the *intS* locus (Fw:
601 GTACTTACCCCGCACTCCAT, Rv: TGTTCAGCACACCAATAGAGG). Next, that kanamycin resistance
602 cassette was removed using pCP20. The resulting markerless strains were further modified by P1
603 transduction with the *lacI* knock-out strain from the KEIO collection (Baba *et al*, 2006) replacing the
604 *lacI* gene with the kanamycin resistance cassette. The deletion was confirmed by sequencing PCR
605 products generated using primers binding outside the *lacI* locus (Fw: CGGCTCATGGATGGTGTT, Rv:
606 CGAAGCGGCATGCATTTAC). We reasoned, that here a $P_{LlacO-1}$-driven *lacI* allows a better control of
607 the $P_{LlacO-1}$-driven *folA* based on observations in (Kavčič *et al*, 2020; Klumpp *et al*, 2009) dealing with
608 growth rate independent negative autoregulation. Moreover, with the combination of RBS1 and the
609 Lac-repressor driven by P_{lacO1} we achieved expression close to wild-type levels. For the generation of
610 the strains with modified RBS3-6 from BWAA19R1 and BWAA20R1, the kanamycin resistance
611 cassette was removed using pCP20. We again used long reverse primers RBS3-Rv:
612 TCCATGCCGATAACGCGATCTACCGCTAACGCCGCAATCAGACTGATCATGCGGTACCTTTAGGACTCCTCTTT
613 aatgaattcggtcag, RBS4-Rv:
614 TCCATGCCGATAACGCGATCTACCGCTAACGCCGCAATCAGACTGATCATGCGGTACCTTTGTCCTCTTTaatga
615 attcggtcag, RBS5-Rv:
616 TCCATGCCGATAACGCGATCTACCGCTAACGCCGCAATCAGACTGATCATGCGGTACCTTTAGGAGTCCTCTTT

617 aatgaattcggtcag, RBS6-Rv:
618 TCCATGCCGATAACGCGATCTACCGCTAACGCCGCAATCAGACTGATCATGCGGTACCTTTAGGAGGCCTCTTT
619 aatgaattcggtcag, each modified such that the RBS sequence was changed according to (Deris *et al*,
620 2013). To aid primer binding (compare (Liu & Naismith, 2008)) to the template (which carries RBS1
621 sequence) and change of the RBS-sequence (underlined) additional 15 nt were added to the reverse
622 primers (lower case letters) and used in combination with Fw:
623 AACATACCGGCAACATGGCGGATGAACCGGAAACGAAACCCTCATCCTAAGTGTAGGCTGGAGCTGC on
624 pAA39 and pAA40. The respective PCR products were sequenced and used for recombineering of the
625 markerless intermediate versions of BWAA19R1 and BWAA20R1. After integration, all promoter
626 regions were confirmed by sequencing a PCR product obtained with primers targeting the *folA* locus
627 with the primers (Fw: CCAGCGCGATGTTAAGTGA, Rv: GATTGATTCCCAGGTATGGCG).

628 For the recombineering procedure (Datsenko & Wanner, 2000) the temperature-inducible system
629 from pSIM19 (Sharan *et al*, 2009) was used. Chloramphenicol at 10 µg/ml and kanamycin at
630 25 µg/ml were used. During the whole strain construction procedure wherever *folA* was driven by
631 PL_{lacO1}, 1 mM IPTG was added as this inducer controls expression from PL_{lacO1} and *folA* is an essential
632 gene.

633

634 **Mathematical model**

635 Solutions of the mathematical model in Fig. 1B were numerically calculated using Python (function
636 *fsolve* from *scipy* version 1.2.1). As dose-sensitivity without growth-mediated feedback, we used $n =$
637 2 since this is a typical value for many antibiotics (Fig. 1A).

638

639 **Strains and plasmids used in this study**

Name	Information	Source
E. coli BW25113	KEIO collection parent strain (Baba *et al*, 2006)	Lab strain collection
BWAA01	*ΔphoA:kan:*P_{folA}*:gfp* based on P_{folA}-gfp plasmid from (Zaslaver *et al*, 2006)	This study, based on (Bollenbach *et al*, 2009)
BWAA02	*ΔphoA:kan:*P_{folA} based on pUA66 plasmid from (Zaslaver	This study, based on (Bollenbach *et al*, 2009)

	et al, 2006)	
BWAA11	Native regulation *folA:gfp:kan*	This study
BWAA12	Native regulation *folA:kan*	This study
BWAA19R1	IPTG-inducible regulation ΔP_{folA}*:kan:*$P_{LlacO-1}$*:folA:gfp, intS:*$P_{LlacO-1}$*:lacI, ΔlacI:kan*	This study
BWAA19R3	As BWAA19R1 but with RBS3 from (Deris *et al*, 2013)	This study
BWAA19R4	As BWAA19R1 but with RBS4 from (Deris *et al*, 2013)	This study
BWAA19R5	As BWAA19R1 but with RBS5 from (Deris *et al*, 2013)	This study
BWAA19R6	As BWAA19R1 but with RBS6 from (Deris *et al*, 2013)	This study
BWAA20R1	IPTG-inducible regulation ΔP_{folA}*:kan:*$P_{LlacO-1}$*:folA, intS:*$P_{LlacO-1}$*:lacI, ΔlacI:kan*	This study
BWAA20R3	As BWAA20R1 but with RBS3 from (Deris *et al*, 2013)	This study
BWAA20R4	As BWAA20R1 but with RBS4 from (Deris *et al*, 2013)	This study
BWAA20R5	As BWAA20R1 but with RBS5 from (Deris *et al*, 2013)	This study
BWAA20R6	As BWAA20R1 but with RBS6 from (Deris *et al*, 2013)	This study
BW25141	Cloning strain CGSC#: 7633 with *pir*$^{+}$ from (Datsenko & Wanner, 2000)	Lab strain collection
pSIM19	Recombineering plasmid (Datta *et al*, 2006)	Lab strain collection
pCP20	Source of Flp for excision (Cherepanov & Wackernagel, 1995)	Lab strain collection
pKD13-mutgfp	FRT-flanked *kan*, P_{LlacO1}	Bor Kavcic

pCA24N(-)folA	Source of *folA:chl* (Kitagawa *et al*, 2005)	Lab strain collection
pCA24N(-)	Empty ASKA plasmid (Kitagawa *et al*, 2005)	Lab strain collection
pAAtufB	Modified pCA24N(-)tufB	This study
pAA30	Modified pCA24N(-)	This study
pAA39	*folA:gfp:chl* in pKD13-mutgfp	This study
pAA40	*folA:chl* in pKD13-mutgfp	This study
pCS-λ	Luciferase genes for luminescence measurements, *kan*	Ref. (Kishony & Leibler, 2003)

Acknowledgements

This work was in part supported by Human Frontier Science Program Grant RGP0042/2013, Marie Curie Career Integration Grant 303507, Austrian Science Fund (FWF) Grant P 27201-B22, and German Research Foundation (DFG) Collaborative Research Center (SFB) 1310 to Tobias Bollenbach. S. Andreas Angermayr was supported by the European Union's Horizon 2020 research and innovation program under the Marie Skłodowska-Curie grant agreement No 707352. We would like to thank the Bollenbach group for regular fruitful discussions. We are particularly thankful for technical assistance of Booshini Fernando and for discussions of the theoretical aspects with Gerrit Ansmann. We are indebted to Bor Kavčič for invaluable advice, help with setting up the luciferase-based growth monitoring system, and for sharing plasmids. We are grateful to Rosalind Allen, Bor Kavčič , Karin Mitosch and Dor Russ for feedback on the manuscript.

We declare that there are no conflicts of interest.

SAA, GC, and TB conceived the study. SAA and TB designed the experiments. SAA performed the experiments and analyzed the data. GC analyzed data presented in Fig. 1C and Supplementary Fig. 1. SAA and TB wrote the manuscript with input from GC.

References

Baba T, Ara T, Hasegawa M, Takai Y, Okumura Y, Baba M, Datsenko KA, Tomita M, Wanner BL, Mori H, Anderson R, Roth J, Baudin A, Ozier-Kalogeropoulos O, Denouel A, Lacroute F, Cullin C, Blattner F, Plunkett G, Bloch C, et al (2006) Construction of Escherichia coli K-12 in-frame, single-gene knockout mutants: the Keio collection. *Mol. Syst. Biol.* **2:** 2006.0008

662 Balaban NQ, Merrin J, Chait R, Kowalik L & Leibler S (2004) Bacterial persistence as a phenotypic
663 switch. *Science* **305:** 1622–5 Available at:
664 http://www.sciencemag.org/cgi/doi/10.1126/science.1099390 [Accessed January 20, 2014]

665 Baym M, Lieberman TD, Kelsic ED, Chait R, Gross R, Yelin I & Kishony R (2016) Spatiotemporal
666 microbial evolution on antibiotic landscapes. *Science* **353:** 1147–51 Available at:
667 http://www.sciencemag.org/cgi/doi/10.1126/science.aag0822

668 Bershtein S, Choi J-M, Bhattacharyya S, Budnik B & Shakhnovich E (2015) Systems-level response to
669 point mutations in a core metabolic enzyme modulates genotype-phenotype relationship. *Cell*
670 *Rep.* **11:** 645–56 Available at: http://dx.doi.org/10.1016/j.celrep.2015.03.051

671 Bershtein S, Mu W, Serohijos AWR, Zhou J & Shakhnovich EI (2013) Protein Quality Control Acts on
672 Folding Intermediates to Shape the Effects of Mutations on Organismal Fitness. *Mol. Cell* **49:**
673 133–144 Available at: http://dx.doi.org/10.1016/j.molcel.2012.11.004

674 Bhattacharyya S, Bershtein S, Yan J, Argun T, Gilson AI, Trauger SA & Shakhnovich EI (2016) Transient
675 protein-protein interactions perturb E. coli metabolome and cause gene dosage toxicity. *Elife* **5:**
676 1–22 Available at: http://www.ncbi.nlm.nih.gov/pubmed/27938662

677 Bintu L, Buchler NE, Garcia HG, Gerland U, Hwa T, Kondev J, Phillips R, Kuhlman T & Phillips R (2005)
678 Transcriptional regulation by the numbers: models. *Curr. Opin. Genet. Dev.* **15:** 116–24
679 Available at: http://linkinghub.elsevier.com/retrieve/pii/S0959437X05000298

680 Bollenbach T, Quan S, Chait R & Kishony R (2009) Nonoptimal microbial response to antibiotics
681 underlies suppressive drug interactions. *Cell* **139:** 707–18 Available at:
682 http://dx.doi.org/10.1016/j.cell.2009.10.025 [Accessed January 24, 2014]

683 Bremer H & Dennis PP (2008) Modulation of Chemical Composition and Other Parameters of the Cell
684 at Different Exponential Growth Rates. *EcoSal Plus* **3:** 765–77 Available at:
685 http://www.ncbi.nlm.nih.gov/pubmed/26443740

686 Chait R, Craney A & Kishony R (2007) Antibiotic interactions that select against resistance. *Nature*
687 **446:** 668–71 Available at: http://www.ncbi.nlm.nih.gov/pubmed/17410176 [Accessed January
688 24, 2014]

689 Cherepanov PP & Wackernagel W (1995) Gene disruption in Escherichia coli: TcR and KmR cassettes
690 with the option of Flp-catalyzed excision of the antibiotic-resistance determinant. *Gene* **158:** 9–
691 14 Available at: http://www.ncbi.nlm.nih.gov/pubmed/7789817

692 Chevereau G & Bollenbach T (2015) Systematic discovery of drug interaction mechanisms. *Mol. Syst.*
693 *Biol.* **11:** 807 Available at: http://www.ncbi.nlm.nih.gov/pubmed/25924924

694 Chevereau G, Dravecká M, Batur T, Guvenek A, Ayhan DH, Toprak E & Bollenbach T (2015)
695 Quantifying the Determinants of Evolutionary Dynamics Leading to Drug Resistance. *PLoS Biol.*
696 **13:** e1002299 Available at: http://dx.plos.org/10.1371/journal.pbio.1002299

697 Chou T-C & Talalay P (1983) Analysis of combined drug effects: a new look at a very old problem.
698 *Trends Pharmacol. Sci.* **4:** 450–454 Available at:
699 https://linkinghub.elsevier.com/retrieve/pii/016561478390490X

700 Datsenko KA & Wanner BL (2000) One-step inactivation of chromosomal genes in Escherichia coli K-
701 12 using PCR products. *Proc. Natl. Acad. Sci. U. S. A.* **97:** 6640–5

702 Datta S, Costantino N & Court DL (2006) A set of recombineering plasmids for gram-negative
703 bacteria. *Gene* **379:** 109–15 Available at: http://www.ncbi.nlm.nih.gov/pubmed/16750601

704 Deris JB, Kim M, Zhang Z, Okano H, Hermsen R, Groisman A & Hwa T (2013) The innate growth

705 bistability and fitness landscapes of antibiotic-resistant bacteria. *Science* **342:** 1237435
706 Available at: http://www.sciencemag.org/cgi/doi/10.1126/science.1237435 [Accessed January
707 20, 2014]

708 Dong H, Nilsson L & Kurland C (1995) Gratuitous overexpression of genes in Escherichia coli leads to
709 growth inhibition and ribosome destruction. *J. Bacteriol.* **177:** 1497–1504

710 Elf J, Nilsson K, Tenson T & Ehrenberg M (2006) Bistable bacterial growth rate in response to
711 antibiotics with low membrane permeability. *Phys. Rev. Lett.* **97:** 1–4 Available at:
712 http://link.aps.org/doi/10.1103/PhysRevLett.97.258104 [Accessed January 24, 2014]

713 Elowitz MB & Leibler S (2000) A synthetic oscillatory network of transcriptional regulators. *Nature*
714 **403:** 335–338 Available at: http://www.ncbi.nlm.nih.gov/pubmed/10659856

715 Flensburg J & Sköld O (1987) Massive overproduction of dihydrofolate reductase in bacteria as a
716 response to the use of trimethoprim. *Eur. J. Biochem.* **162:** 473–6 Available at:
717 http://www.ncbi.nlm.nih.gov/pubmed/3549289

718 Garcia HG, Lee HJ, Boedicker JQ & Phillips R (2011) Comparison and Calibration of Different
719 Reporters for Quantitative Analysis of Gene Expression. *Biophys. J.* **101:** 535–544

720 Gardner TS, Cantor CR & Collins JJ (2000) Construction of a genetic toggle switch in Escherichia coli.
721 *Nature* **403:** 339–342 Available at:
722 http://www.nature.com/nature/journal/v403/n6767/full/403339a0.html

723 Greulich P, Scott M, Evans MR & Allen RJ (2015) Growth-dependent bacterial susceptibility to
724 ribosome-targeting antibiotics. *Mol. Syst. Biol.* **11:** 796 Available at:
725 http://www.pubmedcentral.nih.gov/articlerender.fcgi?artid=4380930&tool=pmcentrez&rende
726 rtype=abstract [Accessed March 21, 2015]

727 Hansen MT, Pato ML, Molin S, Fill NP & von Meyenburg K (1975) Simple downshift and resulting lack
728 of correlation between ppGpp pool size and ribonucleic acid accumulation. *J. Bacteriol.* **122:**
729 585–91 Available at: http://www.ncbi.nlm.nih.gov/pubmed/1092659 [Accessed September 6,
730 2018]

731 Hansson MD, Rzeznicka K, Rosenbäck M, Hansson M & Sirijovski N (2008) PCR-mediated deletion of
732 plasmid DNA. *Anal. Biochem.* **375:** 373–5 Available at:
733 http://www.ncbi.nlm.nih.gov/pubmed/18157935

734 Heckman KL & Pease LR (2007) Gene splicing and mutagenesis by PCR-driven overlap extension. *Nat.*
735 *Protoc.* **2:** 924–32 Available at: http://www.ncbi.nlm.nih.gov/pubmed/17446874

736 Hermsen R, Deris JB & Hwa T (2012) On the rapidity of antibiotic resistance evolution facilitated by a
737 concentration gradient. *Proc. Natl. Acad. Sci.* **109:** 10775–10780

738 Hol FJH, Hubert B, Dekker C & Keymer JE (2016) Density-dependent adaptive resistance allows
739 swimming bacteria to colonize an antibiotic gradient. *ISME J.* **10:** 30–38 Available at:
740 http://www.nature.com/doifinder/10.1038/ismej.2015.107

741 Kavčič B, Tkačik G & Bollenbach T (2020) Mechanisms of drug interactions between translation-
742 inhibiting antibiotics. *Nat. Commun.* **11:** 4013 Available at:
743 https://www.nature.com/articles/s41467-020-17734-z [Accessed November 17, 2019]

744 Keseler IM (2004) EcoCyc: a comprehensive database resource for Escherichia coli. *Nucleic Acids Res.*
745 **33:** D334–D337 Available at: http://nar.oxfordjournals.org/lookup/doi/10.1093/nar/gki108
746 [Accessed January 20, 2014]

747 Kishony R & Leibler S (2003) Environmental stresses can alleviate the average deleterious effect of

748 mutations. *J. Biol.* **2:** 14 Available at: http://www.jbiol.com/content/2/2/14 [Accessed February
749 21, 2014]

750 Kitagawa M, Ara T, Arifuzzaman M, Ioka-Nakamichi T, Inamoto E, Toyonaga H & Mori H (2005)
751 Complete set of ORF clones of Escherichia coli ASKA library (A complete set of E. coli K-12 ORF
752 archive): unique resources for biological research. *DNA Res.* **12:** 291–299

753 Klumpp S, Zhang Z & Hwa T (2009) Growth rate-dependent global effects on gene expression in
754 bacteria. *Cell* **139:** 1366–75 Available at:
755 http://linkinghub.elsevier.com/retrieve/pii/S0092867409015050 [Accessed January 20, 2014]

756 Lee AJ, Wang S, Meredith HR, Zhuang B, Dai Z & You L (2018) Robust, linear correlations between
757 growth rates and β-lactam-mediated lysis rates. *Proc. Natl. Acad. Sci. U. S. A.* **115:** 4069–4074
758 Available at: http://www.pnas.org/lookup/doi/10.1073/pnas.1719504115

759 Liu H & Naismith JH (2008) An efficient one-step site-directed deletion, insertion, single and
760 multiple-site plasmid mutagenesis protocol. *BMC Biotechnol.* **8:** 91 Available at:
761 http://bmcbiotechnol.biomedcentral.com/articles/10.1186/1472-6750-8-91

762 Lutz R & Bujard H (1997) Independent and tight regulation of transcriptional units in Escherichia coli
763 via the LacR/O, the TetR/O and AraC/I1-I2 regulatory elements. *Nucleic Acids Res.* **25:** 1203–10

764 Mitosch K, Rieckh G & Bollenbach T (2017) Noisy Response to Antibiotic Stress Predicts Subsequent
765 Single-Cell Survival in an Acidic Environment. *Cell Syst.* **4:** 393-403.e5 Available at:
766 http://www.ncbi.nlm.nih.gov/pubmed/28342718

767 Nichols RJ, Sen S, Choo YJ, Beltrao P, Zietek M, Chaba R, Lee S, Kazmierczak KM, Lee KJ, Wong A,
768 Shales M, Lovett S, Winkler ME, Krogan NJ, Typas A & Gross CA (2011) Phenotypic landscape of
769 a bacterial cell. *Cell* **144:** 143–56 Available at:
770 http://linkinghub.elsevier.com/retrieve/pii/S0092867410013747 [Accessed January 23, 2014]

771 Nyerges Á, Csörgő B, Draskovits G, Kintses B, Szili P, Ferenc G, Révész T, Ari E, Nagy I, Bálint B,
772 Vásárhelyi BM, Bihari P, Számel M, Balogh D, Papp H, Kalapis D, Papp B & Pál C (2018) Directed
773 evolution of multiple genomic loci allows the prediction of antibiotic resistance. *Proc. Natl.*
774 *Acad. Sci. U. S. A.* **115:** E5726–E5735 Available at:
775 http://www.ncbi.nlm.nih.gov/pubmed/29871954%0Ahttp://www.pnas.org/lookup/doi/10.107
776 3/pnas.1801646115

777 Palmer AC & Kishony R (2014) Opposing effects of target overexpression reveal drug mechanisms.
778 *Nat. Commun.* **5:** 4296 Available at: http://www.ncbi.nlm.nih.gov/pubmed/24980690
779 [Accessed July 2, 2014]

780 Regoes RR, Wiuff C, Zappala RM, Garner KN, Baquero F & Levin BR (2004) Pharmacodynamic
781 functions: a multiparameter approach to the design of antibiotic treatment regimens.
782 *Antimicrob. Agents Chemother.* **48:** 3670–6 Available at:
783 http://www.ncbi.nlm.nih.gov/pubmed/15388418

784 Rodrigues J V, Bershtein S, Li A, Lozovsky ER, Hartl DL & Shakhnovich EI (2016) Biophysical principles
785 predict fitness landscapes of drug resistance. *Proc. Natl. Acad. Sci. U. S. A.* **113:** E1470-8
786 Available at: http://www.pnas.org/lookup/doi/10.1073/pnas.1603613113

787 Rood JI, Laird AJ & Williams JW (1980) Cloning of the Escherichia coli K-12 dihydrofolate reductase
788 gene following mu-mediated transposition. *Gene* **8:** 255–65 Available at:
789 http://www.ncbi.nlm.nih.gov/pubmed/6444603

790 Russ D & Kishony R (2018) Additivity of inhibitory effects in multidrug combinations. *Nat. Microbiol.*
791 **3:** 1339–1345 Available at: http://www.ncbi.nlm.nih.gov/pubmed/30323252

792 Scott M, Gunderson CW, Mateescu EM, Zhang Z & Hwa T (2010) Interdependence of cell growth and
793 gene expression: origins and consequences. *Science* **330:** 1099–102 Available at:
794 http://science.sciencemag.org/content/330/6007/1099.long

795 Sharan SK, Thomason LC, Kuznetsov SG & Court DL (2009) Recombineering: a homologous
796 recombination-based method of genetic engineering. *Nat. Protoc.* **4:** 206–223

797 Soo VWC, Hanson-Manful P & Patrick WM (2011) Artificial gene amplification reveals an abundance
798 of promiscuous resistance determinants in Escherichia coli. *Proc. Natl. Acad. Sci. U. S. A.* **108:**
799 1484–9

800 Toprak E, Veres A, Michel J-B, Chait R, Hartl DL & Kishony R (2012) Evolutionary paths to antibiotic
801 resistance under dynamically sustained drug selection. *Nat. Genet.* **44:** 101–105 Available at:
802 http://www.nature.com/doifinder/10.1038/ng.1034 [Accessed January 20, 2014]

803 Tuomanen E, Cozens R, Tosch W, Zak O & Tomasz A (1986) The rate of killing of Escherichia coli by
804 beta-lactam antibiotics is strictly proportional to the rate of bacterial growth. *J. Gen. Microbiol.*
805 **132:** 1297–304 Available at: http://www.ncbi.nlm.nih.gov/pubmed/3534137

806 Yang J, Ogawa Y, Camakaris H, Shimada T, Ishihama A & Pittard AJ (2007) folA, a New Member of the
807 TyrR Regulon in Escherichia coli K-12. *J. Bacteriol.* **189:** 6080–6084 Available at:
808 https://jb.asm.org/content/189/16/6080

809 Zaslaver A, Bren A, Ronen M, Itzkovitz S, Kikoin I, Shavit S, Liebermeister W, Surette MG & Alon U
810 (2006) A comprehensive library of fluorescent transcriptional reporters for Escherichia coli.
811 *Nat. Methods* **3:** 623–628 Available at: http://www.nature.com/doifinder/10.1038/nmeth895

812

Supplementary figures

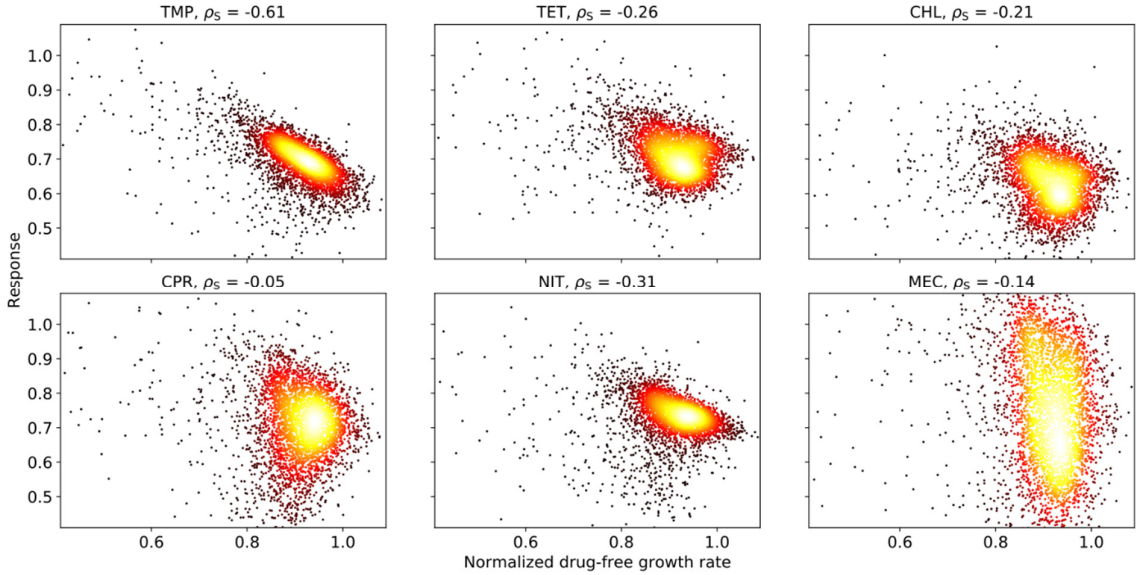

Supplementary Fig. 1|Correlation of antibiotic response and drug-free growth rate for genome-wide gene deletion strains. *Density scatterplots showing growth response to different antibiotics versus normalized growth rate in the absence of drug for genome-wide gene deletion strains* (Baba *et al*, 2006) *as in Fig. 1C. Response is defined as growth rate in the presence of the respective drug normalized to the drug-free growth rate of the respective deletion strain. Each drug was used at a fixed drug concentration that inhibits wild type growth by about 30%* (Chevereau *et al*, 2015). *Spearman correlation coefficient* ρ_S *is shown.*

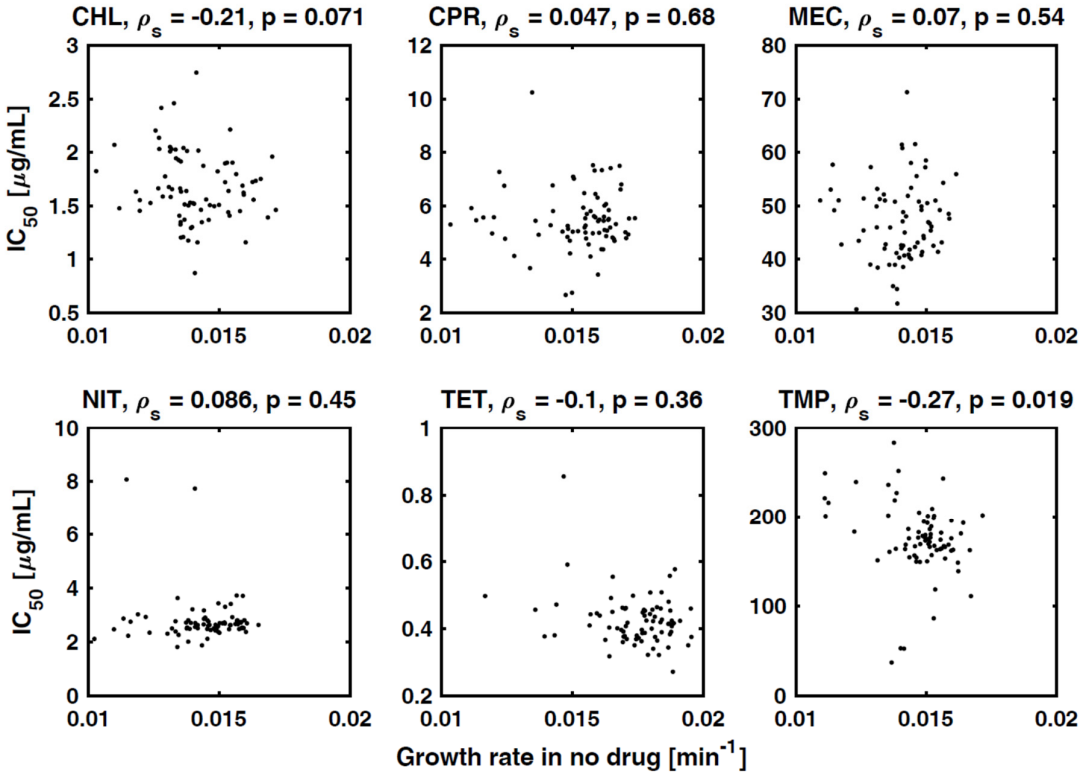

Supplementary Fig. 2|Correlation of IC_{50} and drug-free growth rate in gene deletion strains. *Scatterplots of the IC_{50} of gene deletion mutants versus the growth rate of these mutants in the absence of drug; each panel shows a different antibiotic as labeled. ρ_s is the Spearman correlation; p-values of this correlation are shown. The only significant (negative) correlation occurs for TMP, consistent with growth-mediated negative feedback for this drug. IC_{50}s were determined from dose-response curve measurements of 78 arbitrary gene deletions strains* (Chevereau *et al*, 2015).

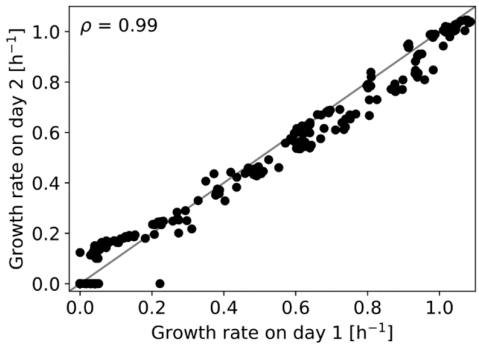

Supplementary Fig. 3| Day-to-day reproducibility of growth rate measurements. *Scatterplot showing comparison of growth rate data from αMG-TMP two-dimensional concentration gradient experiment (Fig. 2B) performed on two different days.*

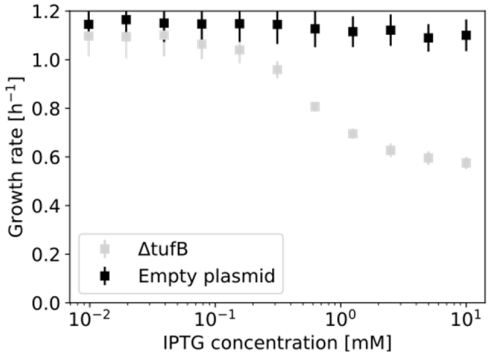

Supplementary Fig. 4| IPTG alone at the concentrations used here has no effect on growth rate. *Black data points show growth rate versus IPTG concentration for a control strain with an empty expression vector; data from Fig. 2C is shown in gray for comparison. Error bars show standard deviation from eight replicates.*

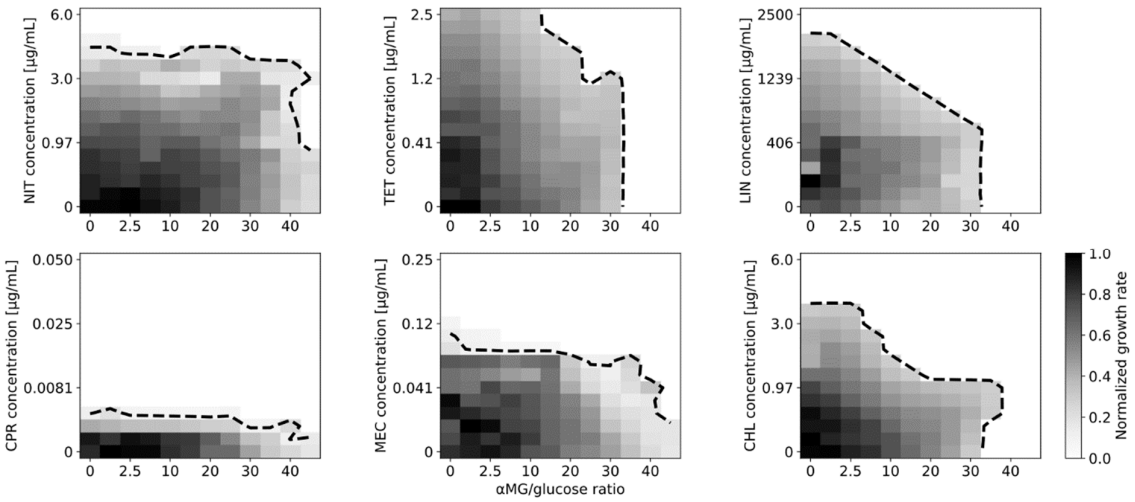

Supplementary Fig. 5| Effect of growth rate reduction by glucose limitation on susceptibility to diverse antibiotics. *As Fig. 2B, for nitrofurantoin (NIT), tetracycline (TET), lincomycin (LIN), ciprofloxacin (CPR), mecillinam (MEC), and chloramphenicol (CHL). Lowering growth rate by glucose limitation via αMG does not lower susceptibility to these antibiotics as for TMP (cf. Fig. 2C).*

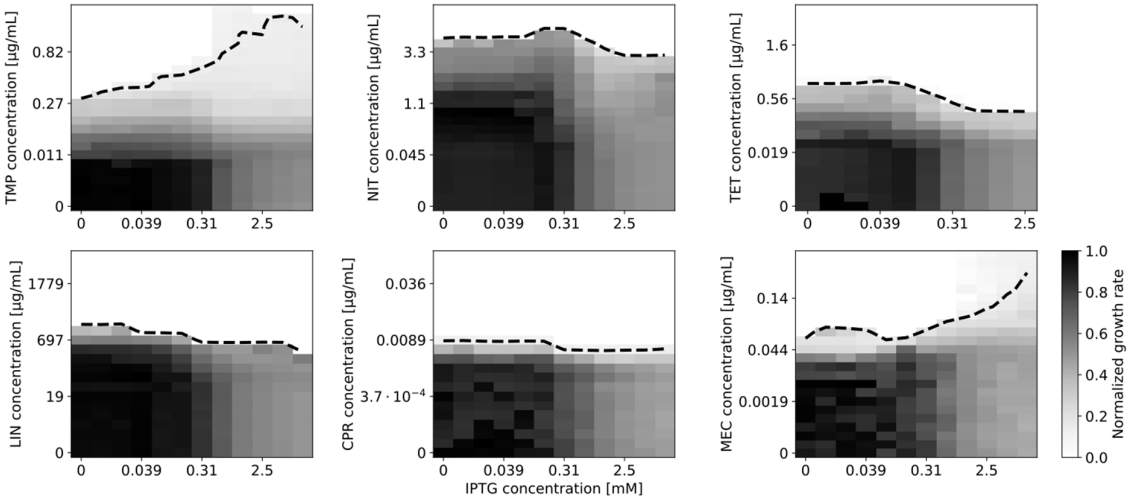

Supplementary Fig. 6| Effect of growth rate reduction by gratuitous protein overexpression on susceptibility to antibiotics. *As Fig. 2E, for trimethoprim (TMP), nitrofurantoin (NIT), tetracycline (TET), lincomycin (LIN), ciprofloxacin (CPR), and mecillinam (MEC). Lowering growth rate by gratuitous protein overexpression lowers susceptibility to TMP and, to a lesser extent, to MEC (bottom right), but not for the other antibiotics (cf. Fig. 2F).*

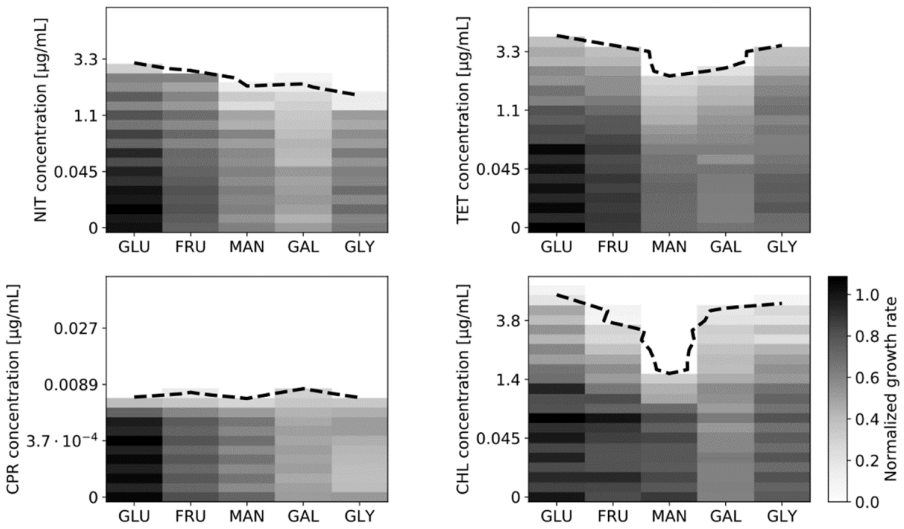

Supplementary Fig. 7| Effect of growth rate reduction by changing carbon source on susceptibility to antibiotics. *As Fig. 2H, for nitrofurantoin (NIT), tetracycline (TET), ciprofloxacin (CPR), and chloramphenicol (CHL). Lowering growth rate via poorer carbon sources does not lower susceptibility to other antibiotics than TMP (cf. Fig. 2I). Data shown is the mean of three replicates. We also performed this assay for mecillinam (MEC), but excluded it from further analysis because – for unknown reasons – it consistently showed extremely noisy dose-response curves in this assay.*

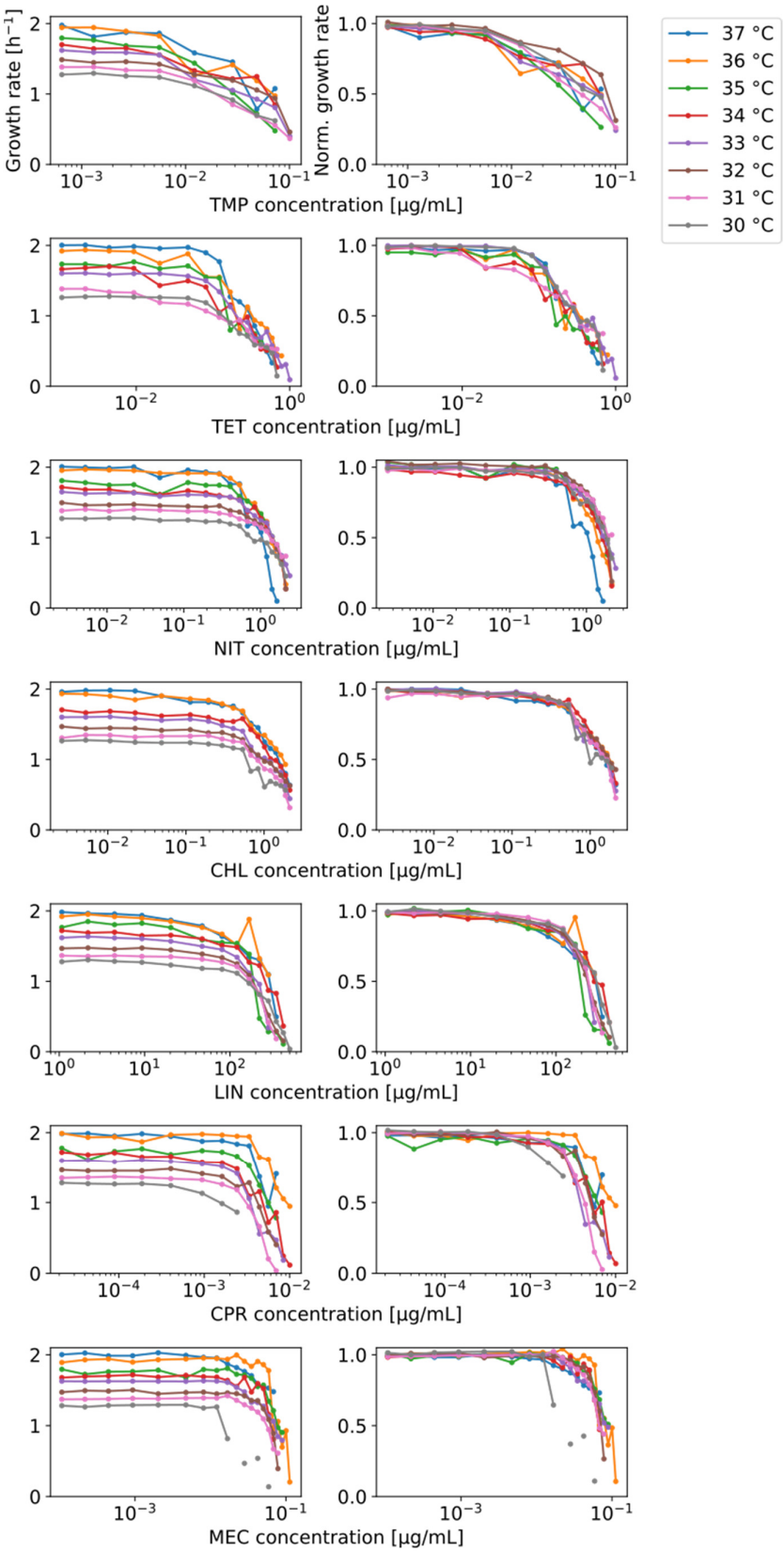

Supplementary Fig. 8|Lowering growth rate by changing temperature does not affect the shape of antibiotic dose-response curves. *Left column: Growth rate versus drug concentration for eight different antibiotics at eight different temperatures as shown. Right column: Growth rate normalized to drug-free growth rate.*

856

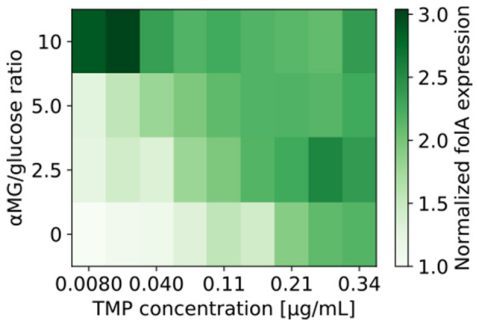

857

858 ***Supplementary Fig. 9|Expression level of folA as a function of trimethoprim and αMG/glucose ratio.*** *Data from Fig. 2 in*
859 *two-dimensional checkerboard plot.*

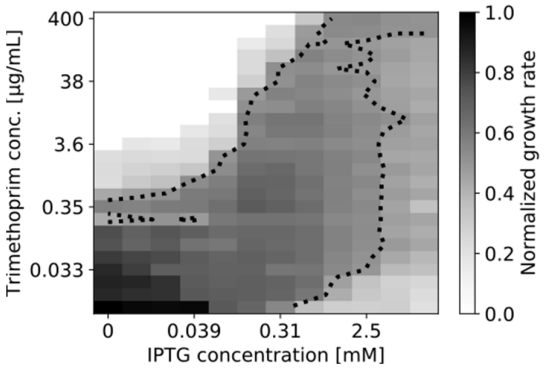

Supplementary Fig. 10|Growth rate decrease due to DHFR overexpression is rescued by trimethoprim. *Normalized growth rate (gray scale) in a two-dimensional concentration gradient of IPTG and TMP. IPTG controls overexpression of folA (Methods). Dotted lines are contour lines at 50% growth inhibition. DHFR overexpression lowers growth rate but adding TMP at high IPTG concentrations partially rescues this phenotype: Growth rate increases with increasing TMP concentration. The increase in TMP* IC_{50} *resulting from DHFR overexpression confirms previous reports* (Palmer & Kishony, 2014).

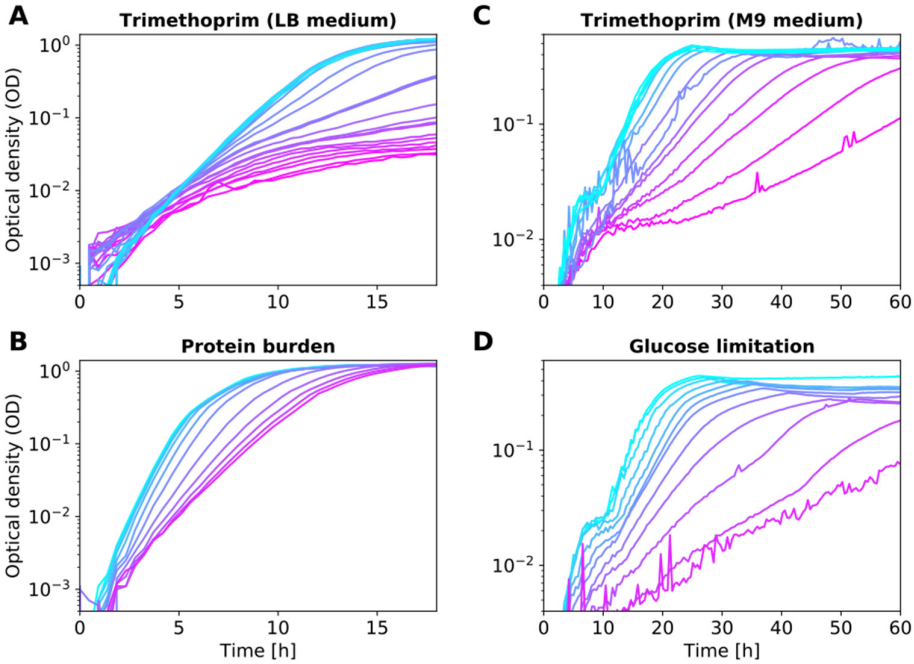

868

869 ***Supplementary Fig. 11| Bacterial growth curves from optical density measurements.*** *Representative data for different*
870 *ways of lowering the growth rate in different growth media.* ***(A)*** *TMP in LB medium. Growth curves underlying the data*
871 *shown in the leftmost column of Fig. 2E; TMP concentration increases from cyan to magenta.* ***(B)*** *Gratuitous protein*
872 *overexpression in LB medium; data correspond to Fig. 2D; IPTG concentration increases from cyan to magenta.* ***(C)*** *TMP in*
873 *glucose (minimal M9) medium; data correspond to the leftmost column of Fig. 2B.* ***(D)*** *αMG in glucose (minimal M9)*
874 *medium; data correspond to Fig. 2A; αMG/glucose ratio increases from cyan to magenta.*